Direct kinetic fingerprinting and digital counting of single protein molecules

Tanmay Chatterjee[a], Achim Knappik[b], Erin Sandford[c], Muneesh Tewari[c], Sung Won Choi[d], William B. Strong[e], Evan P. Thrush[e], Kenneth J. Oh[e], Ning Liu[e,1], Nils G. Walter[a,1], and Alexander Johnson-Buck[a,c,1]

[a]Single Molecule Analysis Group, Department of Chemistry, University of Michigan, Ann Arbor, MI 48109-1055; [b]Life Science Group, Antibodies Division, Bio-Rad AbD Serotec GmbH, 82178 Puchheim, Germany; [c]Department of Internal Medicine, Division of Hematology/Oncology, University of Michigan, Ann Arbor, MI 48109-1055; [d]Department of Pediatrics, Division of Hematology/Oncology, University of Michigan, Ann Arbor, MI 48109-1055; and [e]Life Science Group, Bio-Rad Laboratories, Inc., Hercules, CA 94547

Edited by Joseph D. Puglisi, Stanford University School of Medicine, Stanford, CA, and approved August 5, 2020 (received for review April 28, 2020)

The sensitive and accurate quantification of protein biomarkers plays important roles in clinical diagnostics and biomedical research. Sandwich ELISA and its variants accomplish the capture and detection of a target protein via two antibodies that tightly bind at least two distinct epitopes of the same antigen and have been the gold standard for sensitive protein quantitation for decades. However, existing antibody-based assays cannot distinguish between signal arising from specific binding to the protein of interest and nonspecific binding to assay surfaces or matrix components, resulting in significant background signal even in the absence of the analyte. As a result, they generally do not achieve single-molecule sensitivity, and they require two high-affinity antibodies as well as stringent washing to maximize sensitivity and reproducibility. Here, we show that surface capture with a high-affinity antibody combined with kinetic fingerprinting using a dynamically binding, low-affinity fluorescent antibody fragment differentiates between specific and nonspecific binding at the single-molecule level, permitting the direct, digital counting of single protein molecules with femtomolar-to-attomolar limits of detection (LODs). We apply this approach to four exemplary antigens spiked into serum, demonstrating LODs 55- to 383-fold lower than commercially available ELISA. As a real-world application, we establish that endogenous interleukin-6 (IL-6) can be quantified in 2-μL serum samples from chimeric antigen receptor T cell (CAR-T cell) therapy patients without washing away excess serum or detection probes, as is required in ELISA-based approaches. This kinetic fingerprinting thus exhibits great potential for the ultrasensitive, rapid, and streamlined detection of many clinically relevant proteins.

biomarker detection | single-molecule fluorescence | kinetic fingerprinting | total internal reflection microscopy | superresolution microscopy

Protein and polypeptide biomarkers are widely used to differentiate between healthy and diseased states in both clinical and research settings (1). In addition to such long-standing diagnostic biomarkers as prostate-specific antigen (PSA) (2) and the liver injury-associated enzymes ALT and AST (3), protein biomarkers are increasingly sought for the early detection of disease through noninvasive approaches such as liquid biopsies of cancer (4) or serum-based detection of neurodegenerative disease (5). For example, the CancerSEEK panel detects eight common cancer types via a blood test that measures a combination of circulating tumor DNA mutations and eight protein biomarkers (6). Due to the often low (e.g., femtomolar or subfemtomolar) concentrations of protein biomarkers at the earliest stages of disease, sensitive analytical techniques are required to detect and quantify them.

While subfemtomolar limits of detection (LODs) are readily achieved for many DNA and RNA biomarkers due to the availability of PCR and related techniques, no such amplification is possible for protein analytes. The most sensitive and specific immunoassays tend to utilize a "sandwich" assay format, in which the analyte is captured at a surface by one antibody and detected through the binding of a second antibody, the latter often conjugated to an enzymatic developing reagent for signal amplification and detection by ELISA. However, to achieve maximal sensitivity and reproducibility, these assays—developed almost 50 y ago (7)—require stringent washing to remove excess reagents, as well as the availability of at least two antibodies that bind different epitopes on the same antigen with both high affinity and high specificity. Even with stringent washing and high-quality antibodies, however, nonspecific binding of probes to the assay surface and/or spontaneous conversion of the chromogenic substrate produce nonnegligible levels of background signal (8). Consequently, conventional ELISAs often fail to reliably achieve LODs below 1 pM (10^{-12} M), which may render many potentially useful biomarkers analytically inaccessible. Indeed, 9 of the 39 candidate protein biomarkers examined in the CancerSEEK study were present in concentrations at or below the LOD of the commercially available assays in at least 50% of the samples

Significance

The sensitive measurement of specific protein biomarkers is important for medical diagnostics and research. However, existing methods for quantifying proteins use antibody probes that cannot distinguish between specific and nonspecific binding, limiting their sensitivity and specificity. This work establishes a method for distinguishing between specific binding to the target protein and nonspecific binding to assay surfaces using single-molecule kinetic measurements with dynamically binding probes. This is significant because it permits extremely sensitive protein measurements without requiring a high-affinity detection antibody or any washing steps, enabling streamlined and sensitive quantification of proteins even when no pair of high-quality, tightly binding antibodies is available.

Author contributions: M.T., W.B.S., E.P.T., K.J.O., N.L., N.G.W., and A.J.-B. designed research; T.C. and A.J.-B. performed research; A.K. contributed new reagents/analytic tools; T.C. and A.J.-B. analyzed data; T.C., A.K., E.S., M.T., S.W.C., W.B.S., E.P.T., K.J.O., N.L., N.G.W., and A.J.-B. wrote the paper; and S.W.C. supervised the clinical research protocol, informed consent, and regulatory approvals for obtaining clinical specimens from CAR-T patients.

Competing interest statement: The University of Michigan and Bio-Rad Laboratories, Inc. have filed patent applications on technologies described herein, on which M.T., W.B.S, E.P.T., K.J.O., N.L., N.G.W., and A.J.-B. are listed as inventors. M.T., N.G.W., and A.J.-B. are co-founders of aLight Sciences, which sponsored this work and seeks to commercialize the SiMREPS technology. A.K., W.B.S., E.P.T., K.J.O., and N.L. are full-time employees of Bio-Rad Laboratories, Inc., which co-sponsored this work.

This article is a PNAS Direct Submission.

[1]To whom correspondence may be addressed. Email: ning_liu@bio-rad.com, nwalter@umich.edu, or alebuck@umich.edu.

This article contains supporting information online at https://www.pnas.org/lookup/suppl/doi:10.1073/pnas.2008312117/-/DCSupplemental.

First published August 31, 2020.

assayed, precluding their development into potentially informative biomarkers (6).

In the past decade, platforms such as Simoa (9, 10) and Erenna (11) have exploited single-molecule detection to achieve LODs in the low-femtomolar and attomolar range for protein analytes. These are essentially digital versions of a sandwich immunoassay, and achieve single-molecule analyte detection by either carrying out the enzymatic amplification step in femtoliter-sized wells (Simoa) or fluorescence detection of an eluted probe under capillary flow (Erenna). While offering dramatic improvements in sensitivity over conventional ELISA, Simoa and Erenna still require two high-affinity and high-specificity antibodies together with stringent washing to remove excess reagent and necessitate more complex sample handling than traditional immunoassays. Furthermore, as in conventional ELISA, false positives can arise from detection antibodies that bind nonspecifically to assay surfaces, in practice giving LODs orders of magnitude above the levels achievable in the digital detection of nucleic acids (12). Although passivation methods have been developed to reduce the nonspecific binding of proteins to assay surfaces (13–15), nontrivial levels of nonspecific binding are still evident when methods with single-molecule sensitivity are employed (14).

We recently introduced a distinct approach for the digital detection of single nucleic acid molecules, termed SiMREPS (single-molecule recognition through equilibrium Poisson sampling), that leverages transiently binding detection probes to generate kinetic fingerprints (16). SiMREPS monitors the repetitive binding of fluorescently labeled probes to the same molecular copy of a surface-immobilized analyte to achieve extremely high-confidence detection of that single analyte molecule without any enzymatic amplification, and with 99.99999% specificity for point mutations in a DNA sequence (17). Here, we show that the SiMREPS principle can be extended to the direct detection of single protein molecules by the in vitro selection of probes with sufficiently fast dissociation kinetics for repetitive probing. Since specific and nonspecific binding of the detection antibodies yield distinguishable kinetic patterns, this approach enables the detection of low-femtomolar or subfemtomolar concentrations of four model target proteins in serum with virtually no background signal. Furthermore, because detection probes need not be washed away prior to measurement, SiMREPS can accurately quantify target proteins while avoiding the extensive washing steps required of existing immunoassays after sample addition. Using superresolution data processing, we extend the linear dynamic range to ∼3.5 orders of magnitude and demonstrate the accurate quantification of endogenous biomarker interleukin-6 (IL-6) in serum from chimeric antigen receptor T cell (CAR-T cell) therapy patients at significantly higher sensitivity than a commercial ELISA.

Results

Kinetic Fingerprinting Assay Design and Optimization. To extend the powerful SiMREPS principle to proteins, we herein develop a SiMREPS kinetic fingerprinting approach using two antibodies as probes: a capture antibody with slow dissociation kinetics, typically an IgG, and a low-affinity detection antibody with rapid dissociation kinetics ($K_d \geq 10$ nM, $k_{off} \geq 1$ min^{-1}), typically a monovalent antigen-binding fragment (Fab) (Fig. 1*A*). A Fab consists of the two N-terminal domains of the heavy chain and the complete light chain of IgG; it comprises one antigen-binding site and therefore binds to the antigen in a monovalent fashion. The capture antibody is modified with biotin to permit surface immobilization via a streptavidin bridge to a biotinyl-PEG (polyethylene glycol)-coated coverslip, while the detection Fab is modified with an organic fluorophore to enable detection of its binding near the coverslip surface by total internal reflection fluorescence (TIRF) microscopy (18, 19). Labeling of both antibodies is performed using standard NHS (*N*-hydroxysuccinimide) ester-amine bioconjugation chemistry (20), with an approximate labeling stoichiometry of 1:1 as estimated by spectrophotometric approaches (*Materials and Methods*).

To achieve reproducibly high analytical performance, we optimized our protocols for coverslip modification as well as the composition of the SiMREPS imaging buffer and sample diluent, since we found that the protocols previously developed for SiMREPS of nucleic acids (21) were not sufficient to reduce nonspecific binding of several detection Fabs to tolerable levels (*SI Appendix*, Figs. S1–S6). In particular, reducing the ratio of biotin-PEG:mPEG from the standard ratio of 1:10 to a ratio of 1:100 reduced the nonspecific binding of several detection antibodies to the surface, presumably by lowering the surface density of streptavidin (*SI Appendix*, Figs. S3 and S4). Nevertheless, as in any immunoassay, the detection antibody exhibits some nonspecific binding to the assay surface or to matrix contaminants adsorbed to the surface that is readily apparent upon single-molecule observation. Fortunately, we found that such nonspecific binding typically exhibits kinetics very distinct from repetitive specific binding of the detection Fab to a single analyte molecule, making it readily distinguishable by analysis of the intensity fluctuations of localized fluorescent spots over time (Fig. 1 *A*–*C*). In general, nonspecific binding results in relatively few binding events in the same location, whereas specific binding to the target results in many antibody binding events to the same surface-captured target molecule. Thus, analysis of the number of binding (dark-to-bright transition) and dissociation (bright-to-dark transition) events (N_{b+d}) as well as the median dwell time in the probe-bound state ($\tau_{on,median}$) was used to distinguish single-molecule traces arising from specific versus nonspecific binding through the application of empirically determined thresholds (Fig. 1 *D* and *E*). Notably, without such kinetic filtering, nonspecific binding accounts for the majority of single-molecule traces in an assay for plasminogen activator inhibitor 1 (PAI-1) and would result in hundreds of false positives per field of view (FOV) (Fig. 1*F*). Kinetic filtering reduced the false positives to essentially zero (<1 per FOV) while retaining the majority of true positives, demonstrating the high specificity of single-molecule protein detection by kinetic fingerprinting.

Antibody Selection and Analytical Performance for Four Model Protein Targets. To demonstrate the high sensitivity and generality of this method, we developed SiMREPS assays for four protein targets: PAI-1, IL-6, vascular endothelial growth factor A (VEGF-A), and interleukin-34 (IL-34), and compared their performance to that of ELISA kits from leading immunoassay manufacturers. The candidate detection Fabs were in vitro selected for binding of recombinant human antigens using a variant of phage display, either with or without explicit selection for fast dissociation from the antigen and their kinetics of antigen binding and dissociation characterized by bio-layer interferometry (BLI) (*Materials and Methods*). Screening a total of 23 candidate Fabs against the four target antigens by SiMREPS showed that the most useful probes exhibit rate constants of association in the range of 0.5–5 × 10^6 M^{-1} s^{-1} and rate constants of dissociation in the range of 0.05 to 0.5 s^{-1} in PBS at 25 to 30 °C, corresponding to K_d values of ∼10 to 600 nM (*SI Appendix*, Table S1 and Fig. S7). We also found that detection Fab kinetics could be readily manipulated by adjusting temperature and/or salt concentration (*SI Appendix*, Figs. S8–S10). Overall, 8 out of 23, or 34.8%, of candidate antibodies were successful as SiMREPS probes, whereas the rest failed due to nonoptimal kinetics (e.g., slow binding and/or dissociation kinetics) or high levels of nonspecific binding to the imaging surface. Encouragingly, for the 12 candidate detection Fabs explicitly in vitro selected for fast dissociation kinetics (*SI Appendix*, Table S1), the overall success rate was significantly higher (6/12 = 50%) than

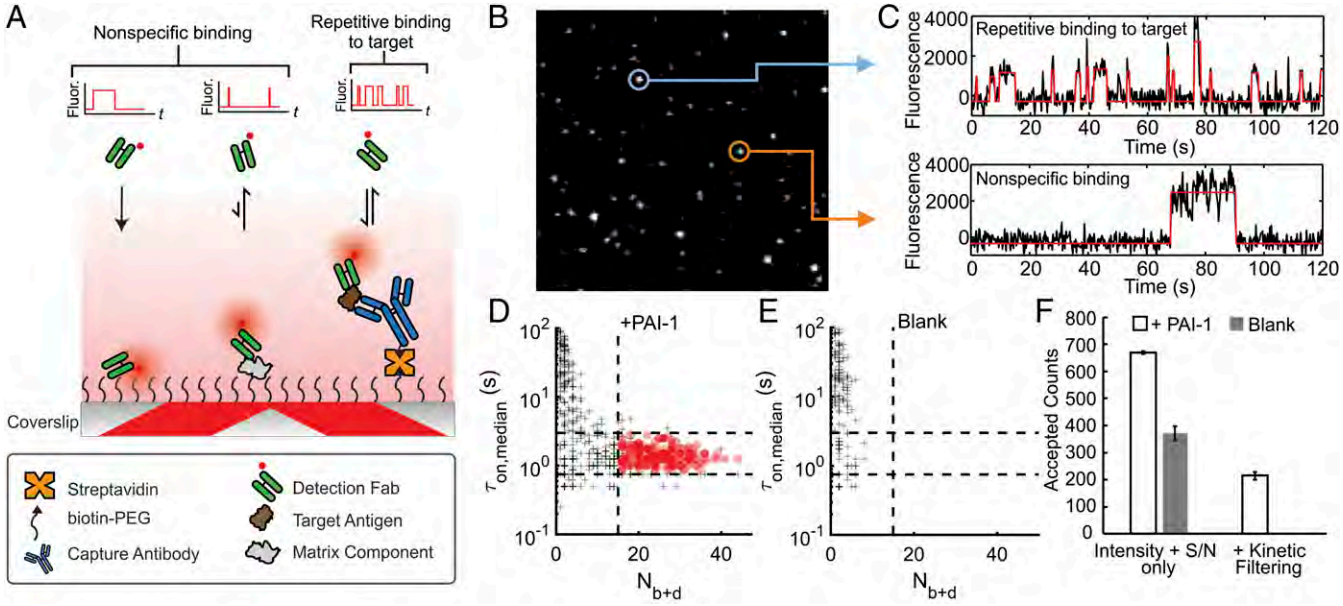

Fig. 1. Detection of single protein molecules by kinetic fingerprinting. (*A*) The interaction of a kinetic fingerprinting probe (detection Fab) with a surface-captured target antigen yields temporal patterns of repeated binding and dissociation, or kinetic fingerprints, distinct from nonspecific interaction of probes with the surface or matrix contaminants. These kinetic fingerprints are measured by TIRF video microscopy. (*B*) Single movie frame of a representative portion of a microscope field of view showing bright puncta at the locations where single fluorescent probes are bound at or near the imaging surface. (*C*) Representative kinetic fingerprints indicative of repetitive binding to the same antigen molecule (*Top*) and nonspecific binding, which is typically less repetitive (*Bottom*). The raw intensity-versus-time traces (black lines) are idealized by hidden Markov modeling (red lines) to extract kinetic parameters for analysis. (*D* and *E*) Scatterplots of N_{b+d} and $\tau_{on,median}$ for all intensity-versus-time trajectories observed within a single field of view in the presence (*D*) or absence (*E*) of target antigen PAI-1 in 25% horse serum. Dashed lines indicate thresholds (minimum or maximum) for accepting a trajectory as evidence of a single PAI-1 molecule. Points indicated by "+" represent trajectories that do not pass filtering for intensity, signal-to-noise, and/or kinetics, and are not considered sufficient evidence to detect PAI-1. Points indicated by red-filled circles represent trajectories that pass filtering and are considered positive detection events of single PAI-1 molecules. (*F*) Impact of kinetic filtering on the number of accepted PAI-1 counts in the presence and absence of spiked-in PAI-1.

for those antibodies not so selected (2/11 = 18.2%), suggesting that the candidate pool can be selectively enriched for promising SiMREPS detection antibodies. Future improvements in surface chemistry—e.g., to further reduce nonspecific probe binding—may permit an even higher success rate of candidate detection Fabs in SiMREPS.

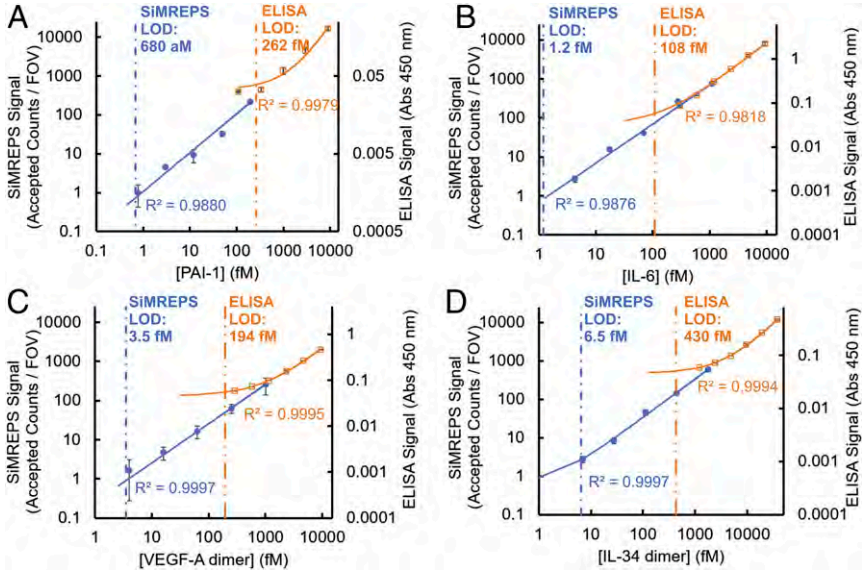

Fig. 2. Quantification of four protein targets using single-molecule kinetic fingerprinting. (*A*–*D*) Standard curves showing quantification of four antigens spiked into 25% serum using SiMREPS (blue closed circles) and conventional sandwich ELISA (orange open squares). Linear regression fits are shown as solid lines. Estimated LODs are indicated as vertical dashed lines for SiMREPS (blue) and sandwich ELISA (orange) and represent median values from at least two standard curves collected on different days. The SiMREPS assays yield LODs 55- to 383-fold lower than the corresponding sandwich ELISAs. Error bars indicate one SD of three (SiMREPS) or two (ELISA) independent measurements.

In each optimized SiMREPS assay, the presence of the antigen resulted in the appearance of a subpopulation of single-molecule traces exhibiting distinctive kinetics of repetitive detection Fab binding in the same location (i.e., kinetic fingerprints), permitting the removal of almost all nonspecific binding signal (*SI Appendix*, Figs. S11 and S12). Both SiMREPS and ELISAs were first performed under controlled conditions with varying concentrations of recombinant antigen spiked into 25% serum (see *Materials and Methods* for details). As shown in Fig. 2, SiMREPS assays exhibit a linear dependence upon analyte concentration, and median LODs ranging from 680 aM to 6.5 fM, considerably below the LODs of 108 to 430 fM observed for the corresponding ELISAs. Interestingly, analysis of the IL-34 standard curve without kinetic filtering yields an LOD of 340 fM (*SI Appendix*, Fig. S13), similar to the measured ELISA LOD of 430 fM and consistent with the notion that the inability to distinguish specific from nonspecific binding of detection antibodies often limits assay sensitivity.

Wash-Free Assay Protocol and Analytical Validation with Clinical Serum Specimens. A common drawback of existing immunoassays is the requirement of multiple washing steps after introduction of the sample, adding to assay complexity and potentially reducing reproducibility. To test whether SiMREPS can be used to circumvent such labor-intensive steps, we developed a wash-free protocol in which a serum sample is simply mixed with the imaging buffer, added to a coverslip coated with capture antibody, and then imaged after a suitable incubation period (Fig. 3*A*). To expand the dynamic range, we also employed a superresolution analysis method that was previously developed for nucleic acid detection with SiMREPS (17), and found that recombinant IL-6 in serum yielded signal that was linearly dependent upon concentration over ∼3.5 orders of magnitude without any washing after sample addition (Fig. 3*B*), in contrast to ∼2 orders of magnitude for diffraction-limited analysis (Fig. 2*B*).

To further test this wash-free protocol and validate SiMREPS for the detection of an endogenous antigen in clinically relevant specimens, we analyzed 34 serum samples from three recipients of CAR-T cell therapy. A common side effect of CAR-T cell therapy is cytokine release syndrome (CRS), a systemic inflammatory response accompanied by a precipitous rise in serum levels of IL-6, a key mediator of CRS (22). As expected, SiMREPS assays revealed a dramatic, persistent rise in IL-6 concentration in serum from a patient with severe CRS (maximum grade = 4); a transient rise in IL-6 concentration in a patient with moderate CRS (maximum grade = 2); and no significant rise in a patient without CRS (Fig. 3*C*). Notably, SiMREPS showed detectable levels of IL-6 in all 34 of the 100-fold diluted serum samples, while ELISA was only able to detect IL-6 in 7/34 of the samples at the same dilution factor (Fig. 3*D*). Performing ELISA of the same serum samples instead at lower dilution (4-fold or 64-fold) yields strong correlation ($R = 0.998$) with the wash-free SiMREPS assay, and the individual patient time courses analyzed by ELISA strongly resemble those measured by SiMREPS (*SI Appendix*, Fig. S14), validating the SiMREPS assay results. It is notable that the expanded dynamic range of SiMREPS with superresolution analysis permitted quantification of IL-6 in all of the clinical samples at the same dilution factor, whereas the ELISA required two different dilution factors to keep IL-6 concentration within the linear dynamic range of the assay. As a more demanding test case, we attempted to detect IL-34—which is not known to rise in CAR-T patient serum—in four serum specimens from patient 6. We found that the high sensitivity of SiMREPS enabled the detection of IL-34 in three of the four specimens, at concentrations well

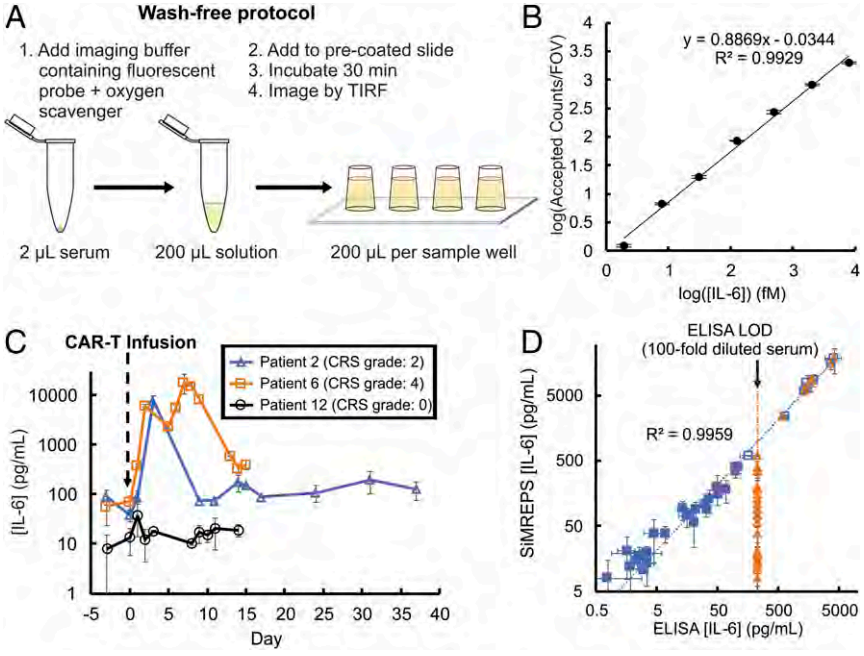

Fig. 3. Wash-free SiMREPS quantification of IL-6 in 100-fold diluted serum samples from CAR-T cell therapy patients. (*A*) Wash-free SiMREPS protocol for quantifying IL-6 in serum. The serum sample containing IL-6 is combined with the imaging solution containing the query probe and then added to a coverslip that was precoated with a capture antibody. After a suitable incubation period (30 min) the sample is imaged by TIRF microscopy to quantify IL-6. A single dilution factor of 100-fold is used for all samples. (*B*) Standard curve from wash-free SiMREPS of IL-6 using superresolution data processing for larger dynamic range. (*C*) Time course of IL-6 concentration as measured by the wash-free SiMREPS protocol in serum samples from three CAR-T therapy patients who experienced a maximum CRS grade of 4 (patient 6, orange squares), 2 (patient 2, blue triangles), or 0 (patient 12, black circles) in response to the therapy during the sample collection window. (*D*) Correlation plot of IL-6 measurements in 34 patient-derived (human) serum samples by SiMREPS (no-wash protocol, 100-fold dilution of all samples) and ELISA with variable dilution factors (4-fold dilution, closed blue squares; 64-fold dilution, open blue squares) or 100-fold dilution of all samples (orange triangles). While SiMREPS detects IL-6 in all 34 samples at 100-fold dilution, sandwich ELISA only detects IL-6 in 7 of 34 samples at the same dilution. Error bars indicate one SD of two independent measurements.

below the LOD of the IL-34 ELISA; furthermore, a corresponding ELISA failed to detect significant levels of IL-34 in any of these specimens (*SI Appendix*, Fig. S15), suggesting that SiMREPS can provide access to analytes too dilute to assay by conventional methods.

Discussion

We here have shown that the kinetic fingerprinting approach of SiMREPS permits distinguishing between specific binding to target proteins and nonspecific binding to assay surfaces and can thus be applied to the counting of single protein molecules with high accuracy. The improved rejection of background binding signal of this method enables quantitative analysis with LODs in the femtomolar-to-attomolar range for four model protein targets spiked into blood serum, corresponding to improvements of 55- to 383-fold relative to commercial ELISAs. We have further shown that SiMREPS can sensitively quantify an endogenous biomarker from only 2 μL of serum, and via superresolution data analysis can achieve a linear dynamic range of about 3.5 orders of magnitude that avoids the need for variable dilution factors when quantifying IL-6 in serum samples from multiple CAR-T patients.

Notably, since nearly all nonspecific binding is filtered out by kinetic analysis, the sensitivity in SiMREPS is limited primarily by the efficiency with which the captured analyte can be imaged. We estimate the overall antigen capture efficiency to be 0.5 to 1.5% for these four assays, and each FOV comprises only ∼0.1% of the total capture area of the sample well, so that each measurement comprising 9 FOVs samples only about 0.01% of the target protein in the mixture. The small size of each FOV (∼100 μm × 100 μm) is due to the high numerical aperture and magnification required in objective-type TIRF. Hence, future improvements in capture efficiency and/or the imaging of larger FOVs are likely to yield consistently subfemtomolar LODs for SiMREPS protein assays. In particular, the use of prism-type TIRF (18) with lower-magnification objectives or large-FOV metalenses (23) may significantly increase the size of each FOV in the specimen plane and lower the LOD proportionally. Despite these sampling limitations, LODs ranging from 0.68 to 6.5 fM were achieved for all four antigens, comparable to the typical LODs for the Simoa platform, albeit not as low as the most sensitive Simoa assays (e.g., as low as 50 aM for PSA in 25% serum) (10).

An attractive feature of SiMREPS is that it can be performed without any washing steps after sample addition, since excess detection probe need not be removed prior to measurement. Thus, it can avoid the labor- and time-intensive washing and sample handling steps of techniques such as ELISA, Simoa, and DNA-PAINT (24). While varying matrix composition could in principle alter the probe binding and/or dissociation kinetics and thereby affect assay performance, the strong correlation ($R^2 > 0.99$) we observe with ELISA measurements of IL-6 in 34 serum specimens from three different patients (Fig. 3*D*) suggests that normal variation in matrix composition has little or no impact on quantification with this wash-free protocol. This lack of complex sample handling should make it easier to adapt SiMREPS to in situ detection and superresolution localization of target antigens in cells and tissues (24) than digital ELISA and related approaches. Other wash-free approaches to protein quantification have been reported recently, including the linker-mediated immunoassay (LMI) (25), nanoswitch-linked immunosorbent assay (NLISA) (26), and an approach to detection of IgG and IgE antibodies using DNA nanoswitches (27). However, none of these approaches achieve the digital detection of single protein molecules, and only NLISA permits LODs in the low-femtomolar range (e.g., LOD of 44 fM for prostate-specific antigen in 20% serum on a single gel lane) (26).

Although the assay workflow of SiMREPS is streamlined compared to ELISA, some developments are necessary before the technique can be widely adopted by biological laboratories. Most importantly, a dedicated, economical, user-friendly SiMREPS instrument would render the approach accessible to those without access to research-grade TIRF microscopes. Indeed, increasingly cheap (28) and user-friendly (29) TIRF microscopes are already available, and these are in most cases overengineered for SiMREPS, which requires only a single illumination geometry (TIRF), one excitation wavelength (e.g., 640 nm), one detection band (e.g., Cy5), and the detection of only enough photons to indicate the presence or absence of a single fluorescent probe. In addition, the development of more user-friendly software that automates the selection of kinetic filtering thresholds in an unsupervised manner from positive and negative control experiments will render data analysis more straightforward.

At the same time, development of detection probes against a larger number of targets will render more biological questions accessible to the technique. Importantly, SiMREPS assays require only one high-affinity probe, which we expect to greatly facilitate the development of new assays, and which may provide access to protein targets for which it is difficult or impossible to find two compatible high-affinity, high-specificity antibodies. In support of this expectation, SiMREPS assays were successfully developed for all four antigens attempted, and one to three suitable detection probes were obtained from each set of four Fabs sourced from in vitro selections tailored to bind in sandwich format and with fast dissociation rates (*SI Appendix*, Table S1). Considering the high success rate we observed in the selection of detection antibodies that achieved highly sensitive detection of all four attempted targets, developing detection probes against additional targets of interest appears quite feasible. Indeed, in vitro screening for high-affinity Fabs using the same fundamental approach as in the present work (30) routinely yields over a dozen clones with fast enough dissociation kinetics ($k_{off} \sim 0.1$–$0.01\ s^{-1}$) to make them promising SiMREPS candidates, but very few that dissociate slowly enough ($k_{off} \sim 1 \times 10^{-4}\ s^{-1}$) to perform well in a conventional ELISA (*SI Appendix*, Fig. S16). In vitro selection and subsequent ELISA testing of purified antibodies can be accomplished in as little as 3 wk with this technology, which is not possible using immunization methods. Moreover, since the most expensive reagents in protein-SiMREPS are the antibodies, and similar quantities of these are used per assay as in ELISA, the cost of materials per assay is comparable to ELISA.

In summary, kinetic fingerprinting with SiMREPS achieves digital detection and counting of single protein molecules without requiring the high-affinity detection antibodies or complex sample handling of conventional sandwich ELISA and related approaches. The SiMREPS principle thus represents a powerful and potentially transformative approach to the highly sensitive quantification of proteins in addition to nucleic acids (16, 17, 31) and small molecules (32).

Materials and Methods

Selection of Detection Fabs. Recombinant Fab antibodies were isolated from the HuCAL PLATINUM library of human antibody genes (33) by two or three iterative rounds of semiautomated panning either on the immobilized antigen or on the complex formed between antigen and the immobilized capture antibody used for SiMREPS. In the latter case, an isotype-matched control antibody was used for blocking of the phage library during panning. For selection and screening, either the standard strategy developed for enrichment of high-affinity antibodies was used (34) (PAI-1 and IL-6), or a modified strategy (for IL-6, IL-34, and VEGF-A) was developed to allow enrichment of clones with high off-rates. In brief, all rounds were performed using hyperphage (35) to enable polyvalent display and therefore avidity-based binding, and washing stringency was decreased in the second and third rounds. After panning, enriched antibody genes were isolated and cloned into an expression vector leading to expression of Fab-FH antibody fragments resulting in monovalent Fab antibodies followed by a FLAG-tag and a His6-tag at the C terminus in tandem. From each panning, 368 clones were randomly picked and grown in microtiter plates. A copy of each plate

was used for Fab expression and ELISA screening on the antigen, the capture antibody, and the complex of antigen bound to capture antibody. A total of 95 ELISA hits from each panning showing binding on antigen and on captured antigen were subjected to a high-throughput off-rate screening as described (30). Clones with highest off-rates were sequenced to identify unique antibodies. In addition, the output of the second panning round for some of the pannings was cloned into an expression vector leading to expression of bivalent Fab-alkaline phosphatase antibody fusion proteins (36) equipped with a FLAG- and a His6-tag. After ELISA screening of the bivalent antibodies, the clones with weak but specific signals were sequenced and unique candidates were converted into monovalent Fab-FH format. For production, *Escherichia coli* TG1F$^-$ cultures (250 mL) containing the chosen antibody genes were grown at 30 °C until OD_{600nm} reached 0.5, and the antibody expression was induced by adding IPTG (isopropyl β-d-1-thiogalactopyranoside) to a final concentration of 1 mM. After further incubation for at least 14 h at 30 °C, the cells were harvested, chemically lysed, and the soluble crude extract was subjected to one-step affinity chromatography (Ni-NTA agarose, Qiagen). After elution of the purified antibodies, the buffer was changed from elution buffer to 1× PBS (phosphate-buffered saline), pH 7.4, and the concentration was determined by UV_{280nm} measurement. Purity and specific activity were tested subsequently by Coomassie-stained SDS-PAGE (sodium dodecyl sulfate–polyacrylamide gel electrophoresis) and ELISA, respectively. Antibodies were stored frozen in PBS buffer.

Affinity Measurements. Kinetic constants were determined by BLI using the ForteBio Octet RED384 instrument essentially as described (30). In brief, each of the purified monovalent Fab antibodies was measured at five concentrations on antigen attached to amine-reactive second generation (AR2G) biosensors. Temperature for measurement was 30 °C. Between measurements the biosensor surfaces were regenerated twice. Association phase was measured for 600 s, dissociation phase typically for 300 s. All measurements were corrected for baseline drift by subtracting a control sensor exposed to running buffer only. Data were analyzed using a 1:1 interaction model on the ForteBio data analysis software (version 7.0.1.5).

Surface Plasmon Resonance (SPR) Analysis. For the two anti-IL-6 antibody clones 29805 and 29806 the dissociation rate constant k_{off} had been determined during the k_{off} ranking, but we did not generate a definitive binding rate constant for these two clones using BLI. We performed the kinetic analysis of these clones in 1× PBS buffer on the ProteOn system (Bio-Rad) following the standard protocol (37). The IL-6 capture antibody at 12.5 μg/mL was immobilized on the ProteOn GLC chip surface through EDAC(1-Ethyl-3-(3-dimethylaminopropyl)carbodiimide)/NHS chemistry at pH 4.5. IL-6 antigen was then applied to the chip surface through six individual channels at the following concentrations: 20 nM, 10 nM, 5 nm, 2.5 nM, 1.25 nM, and 0 nM. The IL-6 antibody clones 29805 or 29806 at 40 nM, 20 nM, 10 nM, 5 nM, 2.5 nM, and 0 nM were applied to the GLC chip to generate the SPR sensorgrams. The antibody's binding to the chip surface was observed for 1 min followed by 5 min of observation of its dissociation from the surface in 1× PBS. Data were analyzed by the ProteOn Manager Software to produce the on- and off-rates for the antibody clones.

Labeling of Detection Fabs. Candidate detection Fabs were fluorescently labeled by amine-NHS ester coupling using Cy5 monoreactive dye packs (GE Healthcare, PA25001). A molar dye:protein ratio of 4:1 to 6:1 was used in labeling reactions, which were carried out in the dark at room temperature for 1 h in 1× PBS, pH 7.2. Antibody-dye conjugates were purified with Ni-NTA (nickel-nitrilotriacetic acid) column chromatography using a wash buffer consisting of 20 mM sodium phosphate, pH 7.4, 500 mM NaCl, and an elution buffer consisting of 20 mM sodium phosphate, pH 7.4, 500 mM NaCl, and 250 mM imidazole. Excess imidazole was removed by overnight dialysis (Slide-A-Lyzer Dialysis Cassette, Thermo Fisher, 3.5K MWCO (molecular weight cut-off) against 1× PBS, pH 7.2, and then aliquoted and frozen at −80 °C. The ratio of dye:protein in the purified detection Fabs was quantified by UV-Vis spectrophotometry (Nanodrop) using the absorbance values at 280 nm and 650 nm and ranged from 0.9:1 to 1.3:1.

Capture Antibodies. Rodent monoclonal IgG capture antibodies had been developed for Bioplex assays previously by Bio-Rad Laboratories, Inc. and were provided as lyophilized powder from a 0.2 μM filtered solution in PBS with 5% trehalose (without carrier bovine serum albumin [BSA]), and biotinylated by amine-NHS ester coupling using biotin-NHS ester (Sigma Aldrich, catalog no. H1759). A molar biotin:IgG ratio of 3:1 to 6:1 was used in labeling reactions, which were carried out at room temperature for 1 h. Biotin-IgG conjugates were purified using Zeba Spin desalting columns (Thermo Fisher, catalog no. 89882, 7K MWCO) according to the manufacturer's recommended protocol, followed by dialysis (Slide-A-Lyzer Dialysis Cassette, Thermo Fisher, 3.5K MWCO) against 1× PBS, pH 7.2. The fraction of biotinylated IgG was estimated by electrophoretic mobility shift assay in the presence or absence of excess streptavidin and ranged from 60 to 80%. The ratio of biotin:IgG, estimated by HABA (4′-hydroxyazobenzene-2-carboxylic acid) assay (38), was ∼1:1. The concentration of biotin-conjugated IgG was estimated from the absorbance at 280 nm using an extinction coefficient of 275,400 M^{-1} cm^{-1} (for IL-6 capture antibody), 259,564 M^{-1} cm^{-1} (for PAI-1 capture antibody), 277,000 M^{-1} cm^{-1} (for VEGF-A capture antibody), and 270,067 M^{-1} cm^{-1} (for IL-34 capture antibody). Capture antibodies were aliquoted and frozen at −80 °C.

Antigens. Recombinant human PAI-1, IL-6, and VEGF-A were provided in lyophilized form by Bio-Rad Laboratories, Inc. Recombinant human IL-34 was purchased from Peprotech (catalog no. 200-34). Antigens were resuspended in 1× PBS, pH 7.4 (Gibco), diluted to a nominal concentration of ∼32 pM in 1× PBS supplemented with 10 mg/mL BSA as a carrier, aliquoted, and frozen at −80 °C. Concentrations of stock solutions postthawing were determined in triplicate by ELISA (Abcam: ab46027, ab213797, and ab119566; and Invitrogen eBioscience: 50-112-5262) according to the manufacturers' recommended protocols, and these estimated concentrations were used in preparing all subsequent dilutions for SiMREPS assays and ELISA comparisons.

Preparation of Slide Surfaces for Single-Molecule Microscopy. Cover glasses (No. 1.5, 24 × 50 mm, VWR no. 48393-241) were functionalized with a 1:100 mixture of biotin-PEG-SVA (succinimidyl valerate) and mPEG-SVA (Laysan Bio, Inc., MPEG-SVA-5000 [1 g] and BIO-PEG-SVA-5K [100 mg]) as previously described (13). We found that using an incubation period of 20 to 24 h in the presence of the PEG reagents rather than the typical 3 h (*SI Appendix*, Fig. S2), using a lower ratio of biotin-PEG-SVA:mPEG-SVA than the typical 1:10 ratio, and blocking unoccupied biotin-binding sites of streptavidin with a secondary addition of biotin-PEG (*SI Appendix*, Fig. S4) yielded superior suppression of nonspecific fluorescent antibody binding (*SI Appendix*, Fig. S5). Coverslips were stored under foil in a nitrogen-purged cabinet until use within 4 wk. Prior to an experiment, four to six sample cells were attached to each coverslip by cutting a ∼2-cm length from the wider end of micropipet tips (Thermo Fisher, no. 02-682-261), discarding the narrower segment of the pipet tip, and then placing the wide end down on the PEGylated coverslip and sealing the edges with epoxy adhesive (Ellsworth Adhesives, no. 4001).

TIRF Microscopy. SiMREPS experiments were performed using one of two Olympus IX-81 objective-type TIRF microscopes equipped with cellTIRF and z-drift control modules (Olympus IX2-ZDC2 or ASI CRISP). While data acquired with the two microscopes are functionally identical, all measurements in a series of replicates or comparison experiments were performed on the same microscope. Detection Fabs were excited in TIRF mode with a theoretical penetration depth of ∼80 nm using a fiber-coupled diode laser (Coherent, Inc. CUBE 640-100C, 100 mW, or OBIS 637 nm LX, 100 mW) with an incident light intensity of ∼100 W/cm^2, and fluorescence emission was detected using an EMCCD (electron-multiplying charge-coupled device: Andor IXon 897, or Photometrics Evolve) with an exposure time of 250 or 500 ms, after passing through a dichroic mirror and emission filter (Chroma, ZT640rdc-UF2 and ET655LP-TRF). In some experiments, an objective heater (Bioptechs) was used to raise the observation temperature to as high as 37 °C (calibrated using the reference thermistor provided by the manufacturer for the specific sample cell geometry used in this study).

Imaging Solution. Unless otherwise specified, all SiMREPS assays were carried out in an imaging solution comprising 1× PBS, pH 7.4; an oxygen scavenger system (39) consisting of 5 mM 3,4-dihydroxybenzoic acid (Fisher, AC114891000), 0.05 mg/mL protocatechuate 3,4-dioxygenase (Sigma-Aldrich, P8279-25UN), and 1 mM Trolox (Fisher, 218940050); 1% Tween 20 (Sigma-Aldrich, P9416-50ML), and 50 nM fluorescent detection Fab. For PAI-1, the buffer was supplemented with NaCl for a total Na^+ concentration of 500 mM.

SiMREPS Assays of Recombinant Antigens. All sample handling was performed in GeneMate low-adhesion 1.7-mL microcentrifuge tubes, and dilutions for standard curves were performed in 25% animal serum (horse serum for IL-6 and PAI-1 spike-ins; chicken serum for VEGF-A and IL-34 spike-ins), 0.75× PBS, pH 7.4, and 7.5 mg/mL BSA. The slide surface was briefly washed with 100 μL of T50 buffer (10 mM Tris·HCl, 50 mM NaCl, 1 mm EDTA (ethylenediaminetetraacetic acid), pH 8.0) followed by the addition of 40 μL 1 mg/mL streptavidin. After 10 min, excess streptavidin was removed, and the sample chamber washed three times with 100 μL of 1× PBS. Next, the capture antibody was immobilized by

adding 40 μL of a solution containing 100 nM of biotinylated capture antibody and 100 nM of biotin-PEG (5 kDa, Laysan Bio, Inc.) in 1× PBS buffer and incubating for 30 min. Excess capture antibody was removed and the sample chamber washed three times with 100 μL of 1× PBS; the last wash was left in the well and not removed until adding the antigen sample. A 100-μL portion of the antigen or blank solution (25% serum) was added to the sample chamber and incubated for 1 h (IL-6, PAI-1) or 3 h (VEGF-A, IL-34) to capture the antigen on the coverslip surface. The sample was removed, the sample cell washed once with 100 μL of 1× PBS, and 100 μL of imaging solution added. Kinetic fingerprints of detection Fab binding were immediately imaged by TIRF microscopy using an acquisition time of 2 min/FOV (IL-6, PAI-1, VEGF-A) or 5 min/FOV (IL-34). An acquisition temperature of 33.5 ± 0.5 °C was used for IL-6, and room temperature (~22 °C) for all other antigens. The LOD was estimated from a linear regression fit of each standard curve by extrapolating the concentration from the signal equal to the mean blank signal plus three SDs of the blank signal. The median LOD from at least three standard curves is reported in Fig. 2.

ELISA Standard Curves. Standard curves for direct comparison with SiMREPS were performed using the same ELISA kits mentioned above (Abcam: ab46027, ab213797, ab119566; and Invitrogen eBioscience: 50-112-5262) according to the manufacturers' recommended protocols, but using the same sample diluent (containing 25% serum) as the SiMREPS assays. The LOD was estimated from a linear regression fit of each standard curve by extrapolating the concentration from the signal equal to the mean blank signal plus three SDs of the blank signal. The median LOD from at least two standard curves is reported in Fig. 2. The manufacturers' claimed LODs for the ELISA kits are: 95 fM (IL-6), 690 fM (PAI-1), 150 fM (VEGF-A), and 190 fM (IL-34).

Wash-Free SiMREPS Standard Curve of IL-6. Capture antibody-coated coverslips were prepared as described under *SiMREPS Assays of Recombinant Antigens*. A 200-μL volume of a mixture containing varying concentrations of recombinant human IL-6 spiked into 2% horse serum, 1× PBS, pH 7.4, 1% Tween 20, 5 mM 3,4-dihydroxybenzoic acid, 0.05 mg/mL protocatechuate 3,4-dioxygenase, 1 mM Trolox, and 50 nM of detection Fab was added to the sample well and incubated for 30 min. Kinetic fingerprints of detection Fab binding were then immediately imaged by TIRF microscopy using an acquisition time of 2 min/FOV at an acquisition temperature of 33.5 °C.

Collection and Handling of CAR-T Patient Serum Samples. Serial serum samples were obtained from three subjects undergoing CAR-T cell therapy. Specimen collection from patients was performed with informed consent. The study was approved by the University of Michigan Institutional Review Board (IRB HUM00115179). Blood was collected in red top Becton Dickinson serum collection tubes and delivered to the laboratory within 2 h of blood draw at room temperature. Serum samples were allowed to clot at room temperature for a minimum of 30 min after blood draw, then centrifuged at 1,200 × *g* for 15 min at room temperature, following which the supernatant was recovered, aliquoted, and immediately frozen and stored at −80 °C. Prior to protein quantification experiments, serum samples were thawed and subjected to centrifugal ultrafiltration (Ultrafree MC, 0.22-μm pore size, Millipore Sigma), then aliquoted and frozen at −80 °C.

Wash-Free Measurement of Endogenous IL-6 in Clinical Serum Samples. Capture antibody-coated coverslips were prepared as described under *SiMREPS Assays of Recombinant Antigens*. A 2-μL portion of each serum sample was added to a separate 198-μL solution to create a mixture containing (all final concentrations in 200 μL total solution): 1× PBS, pH 7.4, 1% Tween 20, 5 mM 3,4-dihydroxybenzoic acid, 0.05 mg/mL protocatechuate 3,4-dioxygenase, 1 mM Trolox, and 50 nM of detection Fab. This 200-μL mixture was added to the sample well and incubated for 30 min. Kinetic fingerprints of detection Fab binding were then immediately imaged by TIRF microscopy using an acquisition time of 2 min/FOV at an acquisition temperature of 33.5 °C.

Measurement of Endogenous IL-34 in Clinical Serum Samples. Serum specimens from patient 6 corresponding to 1, 2, 8, and 15 d after CAR-T infusion were diluted 1:3 in the sample diluent provided with the ELISA kit (Abcam, ab213797) and quantified as instructed by the manufacturer. SiMREPS measurements of 1:3 dilutions of the same serum specimens in the standard diluent (0.75× PBS, pH 7.4, and 7.5 mg/mL BSA) were performed and analyzed as described for the standard curve of recombinant IL-34. LODs for ELISA and SiMREPS were multiplied by 4 to account for the fourfold dilution factor.

Analysis of SiMREPS Data. SiMREPS data were processed using custom MATLAB code to identify sites of fluorescent probe binding and analyze the kinetics of repeated binding as described previously (17, 21). For high-dynamic range measurements (Fig. 3 *B*–*D*), a recently published superresolution approach to data analysis (17) was employed to permit resolution of the more densely captured analyte molecules observed at high concentrations. All other data were analyzed using standard diffraction-limited SiMREPS analysis protocols (21). Briefly, regions of repeated probe binding and dissociation (regions of interest [ROIs]) in the FOV were identified by determining the average absolute frame-to-frame change in intensity at each pixel to create an intensity fluctuation map (21) and then defining ROIs as the 3 × 3 pixel regions centered on local maxima within the fluctuation map. Next, the integrated, background-subtracted intensity within each ROI was calculated for each frame in the movie to generate an intensity-versus-time trace. These candidate traces were subjected to hidden Markov modeling (HMM) using a version of vbFRET (40) with slight modifications to the code to accommodate the varying fluorescence intensities of detection Fabs with different labeling stoichiometries and to interpret these different fluorescent intensities as equivalent (probe bound) states. The idealized trace generated via HMM was used to determine several parameters for SiMREPS kinetic fingerprinting analysis: N_{b+d}, the number of binding and dissociation events; $\tau_{on,median}$ and $\tau_{off,median}$, the median dwell times in the probe-bound and probe-unbound states, respectively; $\tau_{off,max}$, the maximum dwell time in the probe-unbound state; and $r_{s/n}$, the signal-to-noise ratio, defined as the SD of the fluorescence intensity divided by the mean intensity difference between bound and unbound states. Threshold values for each of these parameters to count a trace as a positive detection event of the analyte were optimized by hand for each probe–antigen pair and are shown in *SI Appendix*, Table S2.

Data Availability. Raw microscopy movie files data have been deposited in Deep Blue Data (DOI: https://doi.org/10.7302/na5e-vt32) (41).

ACKNOWLEDGMENTS. This work was funded by aLight Sciences and Bio-Rad Laboratories, Inc.; a University of Michigan Rogel Cancer Center Fund for Discovery Grant in Cellular Cancer Biology Imaging Research; and a Grand Challenge Award from the A. Alfred Taubman Medical Institute. Antibodies, animal serum, and recombinant antigens (except IL-34) were provided by Bio-Rad Laboratories, Inc. SiMREPS analysis software was developed in part using funding from a Michigan Economic Development Corporation MTRAC (Michigan Translational Research and Commercialization) for Life Sciences grant to M.T., N.G.W., and A.J.-B.; as well as NIH grants R21 CA204560 and R33 CA229023 to M.T. and N.G.W. Bio-Rad paid N.G.W. a consulting fee at the outset of the collaboration. We thank Mingde Zhu for performing the SPR kinetics measurements for antibody clones 29806 and 29805; Amanda Mazzoli and Ryan Lindstrom for clinical research coordination of CAR-T study participants; and Jenny Barabas and Mary Olesnavich for technical assistance in specimen processing.

1. J. Simrén, N. J. Ashton, K. Blennow, H. Zetterberg, An update on fluid biomarkers for neurodegenerative diseases: Recent success and challenges ahead. *Curr. Opin. Neurobiol.* **61**, 29–39 (2020).
2. J. Hernández, I. M. Thompson, Prostate-specific antigen: A review of the validation of the most commonly used cancer biomarker. *Cancer* **101**, 894–904 (2004).
3. M. R. McGill, B. L. Woolbright, J. L. Weemhoff, H. Jaeschke, "Mechanistic biomarkers in liver diseases" in *Biomarkers in Disease: Methods, Discoveries and Applications*, V. R. Preedy, Ed. (Springer Netherlands, 2016), pp. 1–27.
4. E. Crowley, F. Di Nicolantonio, F. Loupakis, A. Bardelli, Liquid biopsy: Monitoring cancer-genetics in the blood. *Nat. Rev. Clin. Oncol.* **10**, 472–484 (2013).
5. G. Disanto *et al.*; Swiss Multiple Sclerosis Cohort Study Group, Serum neurofilament light: A biomarker of neuronal damage in multiple sclerosis. *Ann. Neurol.* **81**, 857–870 (2017).
6. J. D. Cohen *et al.*, Detection and localization of surgically resectable cancers with a multi-analyte blood test. *Science* **359**, 926–930 (2018).
7. E. Engvall, P. Perlmann, Enzyme-linked immunosorbent assay (ELISA). Quantitative assay of immunoglobulin G. *Immunochemistry* **8**, 871–874 (1971).
8. L. Cohen, D. R. Walt, Highly sensitive and multiplexed protein measurements. *Chem. Rev.* **119**, 293–321 (2019).
9. D. M. Rissin, D. R. Walt, Digital readout of target binding with attomole detection limits via enzyme amplification in femtoliter arrays. *J. Am. Chem. Soc.* **128**, 6286–6287 (2006).
10. D. M. Rissin *et al.*, Single-molecule enzyme-linked immunosorbent assay detects serum proteins at subfemtomolar concentrations. *Nat. Biotechnol.* **28**, 595–599 (2010).
11. J. Todd *et al.*, Ultrasensitive flow-based immunoassays using single-molecule counting. *Clin. Chem.* **53**, 1990–1995 (2007).
12. C. M. Hindson *et al.*, Absolute quantification by droplet digital PCR versus analog real-time PCR. *Nat. Methods* **10**, 1003–1005 (2013).
13. J. Abelson *et al.*, Conformational dynamics of single pre-mRNA molecules during in vitro splicing. *Nat. Struct. Mol. Biol.* **17**, 504–512 (2010).

14. B. Hua *et al*., An improved surface passivation method for single-molecule studies. *Nat. Methods* **11**, 1233–1236 (2014).
15. D. Y. Joh *et al*., Inkjet-printed point-of-care immunoassay on a nanoscale polymer brush enables subpicomolar detection of analytes in blood. *Proc. Natl. Acad. Sci. U.S.A.* **114**, E7054–E7062 (2017).
16. A. Johnson-Buck *et al*., Kinetic fingerprinting to identify and count single nucleic acids. *Nat. Biotechnol.* **33**, 730–732 (2015).
17. S. L. Hayward *et al*., Ultraspecific and amplification-free quantification of mutant DNA by single-molecule kinetic fingerprinting. *J. Am. Chem. Soc.* **140**, 11755–11762 (2018).
18. D. Axelrod, T. P. Burghardt, N. L. Thompson, Total internal reflection fluorescence. *Annu. Rev. Biophys. Bioeng.* **13**, 247–268 (1984).
19. N. G. Walter, C.-Y. Huang, A. J. Manzo, M. A. Sobhy, Do-it-yourself guide: How to use the modern single-molecule toolkit. *Nat. Methods* **5**, 475–489 (2008).
20. J. S. Nanda, J. R. Lorsch, Labeling a protein with fluorophores using NHS ester derivitization. *Lab. Methods Enzymol. Protein A* **536**, 87–94 (2014).
21. A. Johnson-Buck, J. Li, M. Tewari, N. G. Walter, A guide to nucleic acid detection by single-molecule kinetic fingerprinting. *Methods* **153**, 3–12 (2019).
22. D. W. Lee *et al*., Current concepts in the diagnosis and management of cytokine release syndrome. *Blood* **124**, 188–195 (2014).
23. M. Khorasaninejad *et al*., Metalenses at visible wavelengths: Diffraction-limited focusing and subwavelength resolution imaging. *Science* **352**, 1190–1194 (2016).
24. R. Jungmann *et al*., Multiplexed 3D cellular super-resolution imaging with DNA-PAINT and Exchange-PAINT. *Nat. Methods* **11**, 313–318 (2014).
25. L. D. Smith, M. C. Willard, J. P. Smith, B. T. Cunningham, Development of a linker-mediated immunoassay using chemically transitioned nanosensors. *Anal. Chem.* **92**, 3627–3635 (2020).
26. C. H. Hansen, D. Yang, M. A. Koussa, W. P. Wong, Nanoswitch-linked immunosorbent assay (NLISA) for fast, sensitive, and specific protein detection. *Proc. Natl. Acad. Sci. U.S.A.* **114**, 10367–10372 (2017).
27. A. Porchetta *et al*., Programmable nucleic acid nanoswitches for the rapid, single-step detection of antibodies in bodily fluids. *J. Am. Chem. Soc.* **140**, 947–953 (2018).
28. S. Ramachandran, D. A. Cohen, A. P. Quist, R. Lal, High performance, LED powered, waveguide based total internal reflection microscopy. *Sci. Rep.* **3**, 2133 (2013).
29. Oxford Nanoimager. https://oni.bio/. Accessed 14 January 2020.
30. F. Ylera, S. Harth, D. Waldherr, C. Frisch, A. Knappik, Off-rate screening for selection of high-affinity anti-drug antibodies. *Anal. Biochem.* **441**, 208–213 (2013).
31. X. Su *et al*., Single-molecule counting of point mutations by transient DNA binding. *Sci. Rep.* **7**, 43824 (2017).
32. R. Weng *et al*., Single-molecule kinetic fingerprinting for the ultrasensitive detection of small molecules with aptasensors. *Anal. Chem.* **91**, 1424–1431 (2019).
33. J. Prassler *et al*., HuCAL PLATINUM, a synthetic Fab library optimized for sequence diversity and superior performance in mammalian expression systems. *J. Mol. Biol.* **413**, 261–278 (2011).
34. B. Krebs *et al*., High-throughput generation and engineering of recombinant human antibodies. *J. Immunol. Methods* **254**, 67–84 (2001).
35. S. Rondot, J. Koch, F. Breitling, S. Dübel, A helper phage to improve single-chain antibody presentation in phage display. *Nat. Biotechnol.* **19**, 75–78 (2001).
36. F. Ducancel *et al*., Recombinant colorimetric antibodies: Construction and characterization of a bifunctional F(ab)2/alkaline phosphatase conjugate produced in Escherichia coli. *Biotechnology (N. Y.)* **11**, 601–605 (1993).
37. Bio-Rad Laboratories, Inc., Bulletin 6295: "ProteOn Sensor Chips: Tips and Techniques." (Bio-Rad Laboratories, Inc., Hercules, California, 2012), pp. 1-22. Available at http://www.bio-rad.com/webroot/web/pdf/lsr/literature/Bulletin_6295.pdf. Accessed 13 August 2020.
38. V. G. Janolino, J. Fontecha, H. E. Swaisgood, A spectrophotometric assay for biotin-binding sites of immobilized avidin. *Appl. Biochem. Biotechnol.* **56**, 1–7 (1996).
39. C. E. Aitken, R. A. Marshall, J. D. Puglisi, An oxygen scavenging system for improvement of dye stability in single-molecule fluorescence experiments. *Biophys. J.* **94**, 1826–1835 (2008).
40. J. E. Bronson, J. Fei, J. M. Hofman, R. L. Gonzalez Jr., C. H. Wiggins, Learning rates and states from biophysical time series: A bayesian approach to model selection and single-molecule FRET data. *Biophys. J.* **97**, 3196–3205 (2009).
41. T. Chatterjee *et al*, Dataset (TIRF microscopy movies) for "Direct kinetic fingerprinting and digital counting of single protein molecules." Deep Blue Data. https://doi.org/10.7302/na5e-vt32. Deposited 13 August 2020.

PNAS
www.pnas.org

Supplementary Information for

Direct kinetic fingerprinting and digital counting of single protein molecules

Tanmay Chatterjee[1], Achim Knappik[2], Erin Sandford[3], Muneesh Tewari[3], Sung Won Choi[4], William B. Strong[5], Evan P. Thrush[5], Kenneth J. Oh[5], Ning Liu[5]*, Nils G. Walter[1]** & Alexander Johnson-Buck[1,3]***

[1]Single Molecule Analysis Group, Department of Chemistry, University of Michigan, 930 N. University Ave., Ann Arbor, MI 48109-1055, USA

[2]Bio-Rad AbD Serotec GmbH, Zeppelinstr. 4, 82178 Puchheim, Germany

[3]Department of Internal Medicine, Division of Hematology/Oncology, University of Michigan, 109 Zina Pitcher Pl., Ann Arbor, MI 48109-1055, USA

[4]Department of Pediatrics, Division of Hematology/Oncology, University of Michigan, Ann Arbor, MI 48109-1055, USA

[5]Life Science Group, Bio-Rad Laboratories, Inc., 6000 James Watson Dr., Hercules, CA 94547, USA

* Ning Liu, Nils G. Walter & Alexander Johnson-Buck

Email: *Corresponding author: ning_liu@bio-rad.com

**Corresponding author: nwalter@umich.edu

***Corresponding author: alebuck@umich.edu

This PDF file includes:

Supplementary Figures S1 to S16
Supplementary Tables S1 to S2
SI References

www.pnas.org/cgi/doi/10.1073/pnas.2008312117

Table of Contents

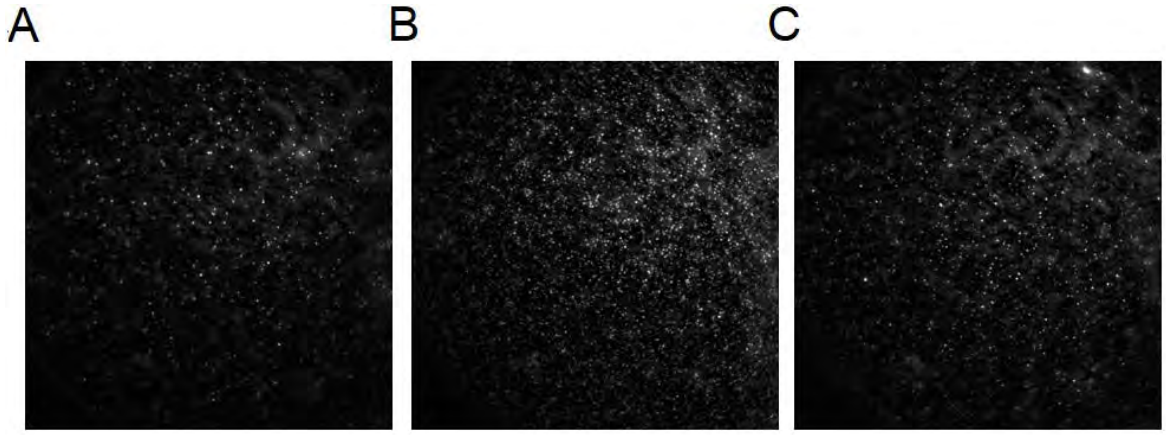

Fig. S1. Influence of coverslip passivation protocol on nonspecific surface binding of kinetic fingerprinting probe for IL-6. a,b,c, Images show the extent of nonspecific binding of 25 nM Cy5-labeled IL-6 detection Fab (clone 29806) to coverslips passivated with (*A*) 1:10 biotin-PEG:mPEG, (*B*) 5 mg/mL biotin-BSA, or (*C*) dichlorodimethylsilane/TWEEN 20 (1). All coverslips were then coated with 1 mg/mL streptavidin (10 min) and 100 nM capture antibody (30 min) followed by incubation with 10 mg/mL BSA in PBS (1 hour) before adding the imaging solution inside. Imaging was conducted at room temperature; images shown are representative 134-µm × 134-µm background-subtracted images from a single movie frame. The biotin-PEG:mPEG passivation method was most effective at suppressing background binding.

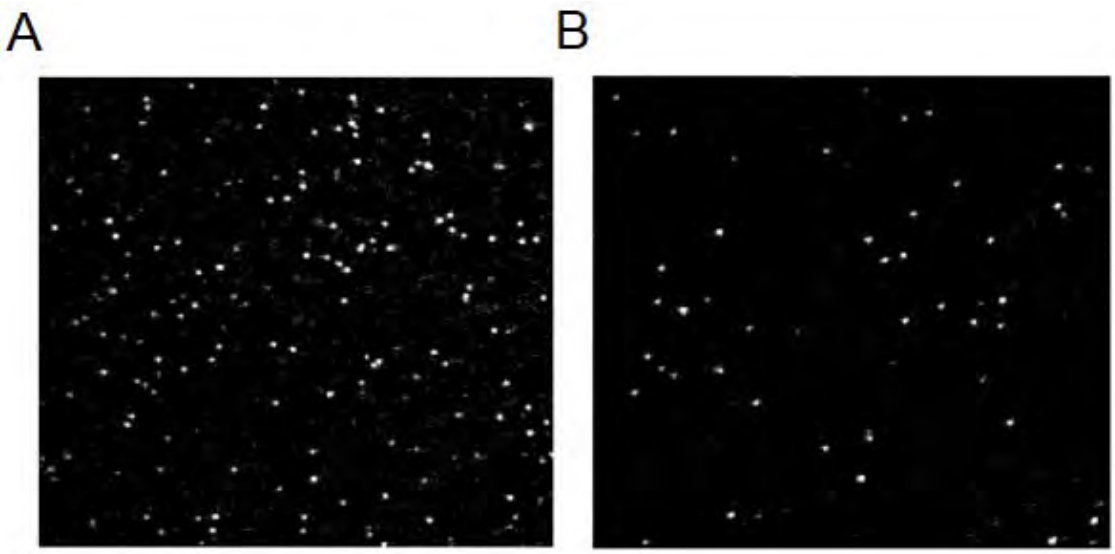

Fig. S2. Effect of incubation time with PEG-NHS ester on the extent of passivation of coverslips against nonspecific detection probe binding. (*A,B)* TIRF microscopy images showing the extent of nonspecific binding of Cy5-labeled IL-6 detection Fabs on coverslips passivated using (*A*) 3-hour or (*B*) 22-hour incubation with 1:10 biotin-PEG-SVA:mPEG-SVA, then coated with streptavidin and biotinylated capture antibody as in the standard protocol. Slides with a longer incubation time in the presence of PEG-NHS esters show improved passivation, so this 22-h incubation time was used for all assays developed in this work. Imaging area shown are 200 × 200-pixel background-subtracted images from representative fields of view.

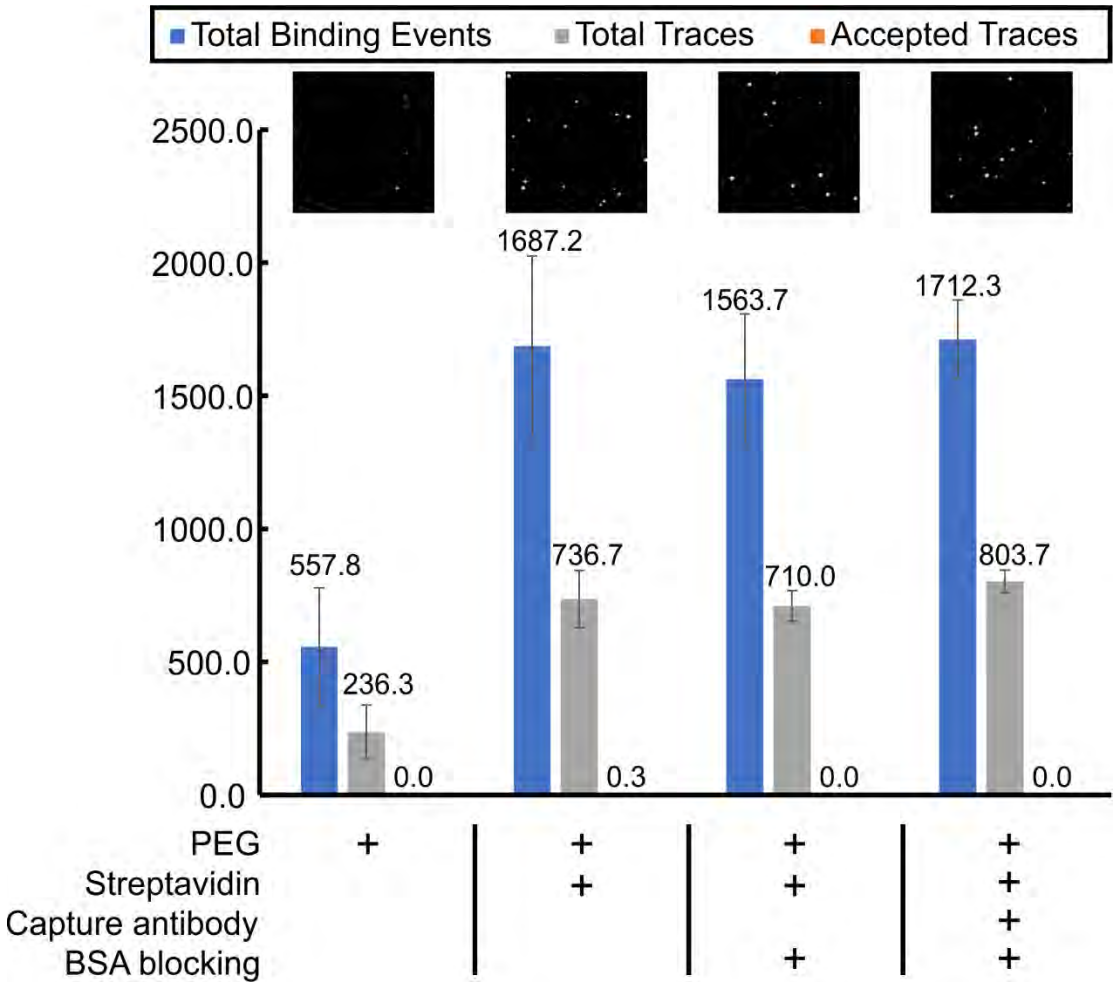

Fig. S3. Influence of streptavidin and capture antibody on nonspecific surface binding of the IL-6 detection Fab (clone 29806). Plotted Cy5 labeled F_{ab} of IL-6 was allowed to interact with a 1:10 biotin-PEG:mPEG-passivated slide surface subsequently treated with different combinations of streptavidin (1 mg/mL, 10 min), capture antibody (100 nM, 30 min), and pre-blocking with BSA (10 mg/mL, 1 h). Plotted are the total number of nonspecific binding events observed within a 134 μm×134 μm FOV (blue bars); the total number of traces selected from the fluctuation map for intensity trace generation (gray bars); and the number of traces (accepted traces) that pass both intensity and kinetic filtering (orange bars; bars not visible, but values range from 0.0 to 0.3). Nonspecific binding to the surface is increased in the presence of streptavidin, with or without the presence of the capture antibody, and BSA blocking does not have a significant impact. Error bars: 1 S.E.M. from 3 replicates.

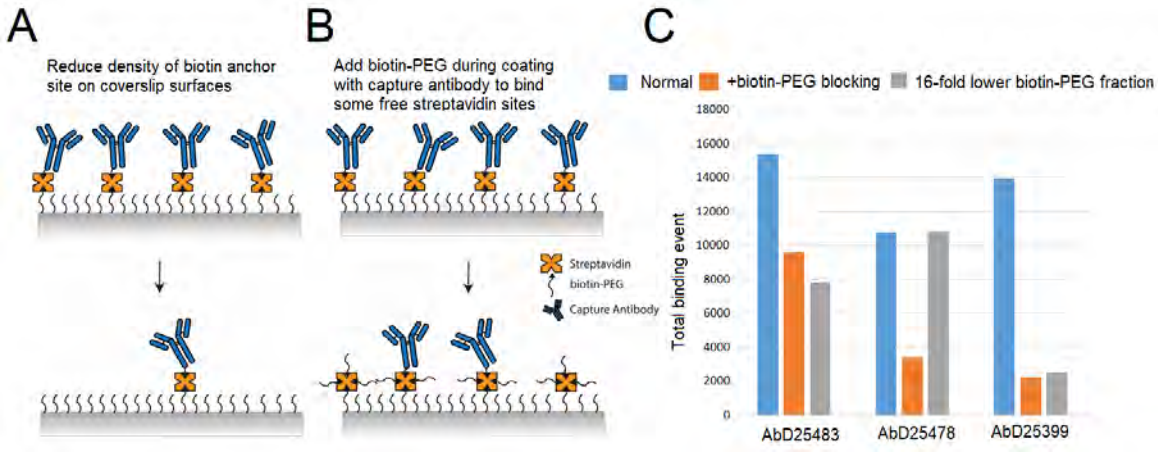

Fig. S4. Evaluating strategies for further suppressing nonspecific binding of detection Fabs to biotin-PEG/mPEG-passivated, streptavidin-modified coverslips. (*A*) Reduction of the density of biotin anchor sites on coverslip surface by lowering the ratio of bio-PEG:mPEG during slide coating, resulting in a lower final density of streptavidin and capture antibody. (*B*) Mixing hydrolysed biotin-PEG-SVA with capture antibody at an equimolar ratio during capture antibody immobilization, blocking exposed streptavidin sites. (*C*) Experimental data showing that the addition of equimolar hydrolyzed biotin-PEG-SVA during capture antibody immobilization (orange bars) and lowering the biotin-PEG-SVA:mPEG-SVA ratio to 1:160 (gray bars) each reduces nonspecific binding for different candidate PAI-1 detection Fabs (AbD25483, AbD25478 and AbD25399) to different extents compared to the original protocol using 1:10 biotin-PEG-SVA:mPEG-SVA (blue bars).

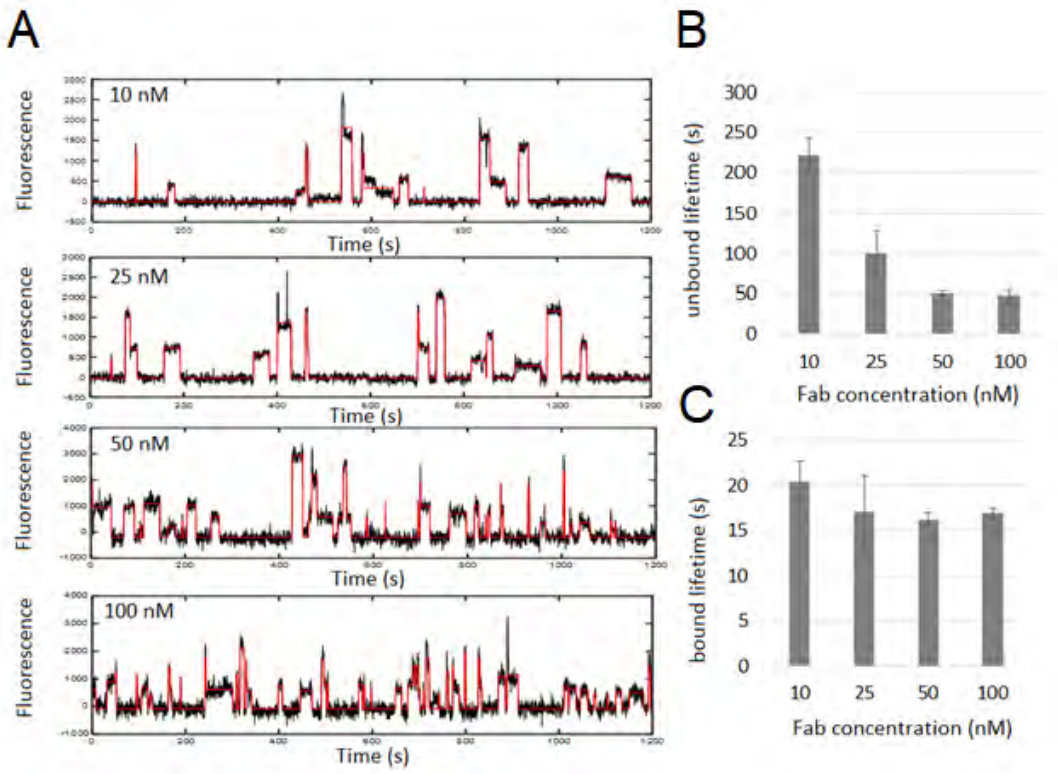

Fig. S5. Impact of varying concentration of IL-6 detection Fab (clone 29806) on signal-to-noise as well as binding and dissociation kinetics. (*A*) Representative single-molecule intensity-*versus*-time traces from TIRF microscopy measurements of the interaction of surface-bound IL-6 with Cy5-labeled detection Fab at varying concentrations: 10 nM, 25 nM, 50 nM, and 100 nM. As the concentration of detection Fab increases, the number of observed binding and dissociation events (N_{b+d}) increases at the cost of a reduced signal-to-noise ratio, particularly at 100 nM. b, c, Apparent lifetime of the unbound (*B*) and bound (*C*) state as a function of detection Fab concentration. The apparent lifetime of the unbound state decreases monotonically up to a concentration of about 50 nM; further increasing the concentration to 100 nM does not decrease the apparent unbound-state lifetime further, suggesting that the antigen may be approaching saturation with detection Fab at 50 nM. Remaining low-fluorescence dwell times may be due to the occupancy of antigen by detection probes lacking an active fluorophore, or the antigen entering a conformational state that is not able to bind the detection probe. As expected, the bound-state lifetime is independent of detection probe concentration.

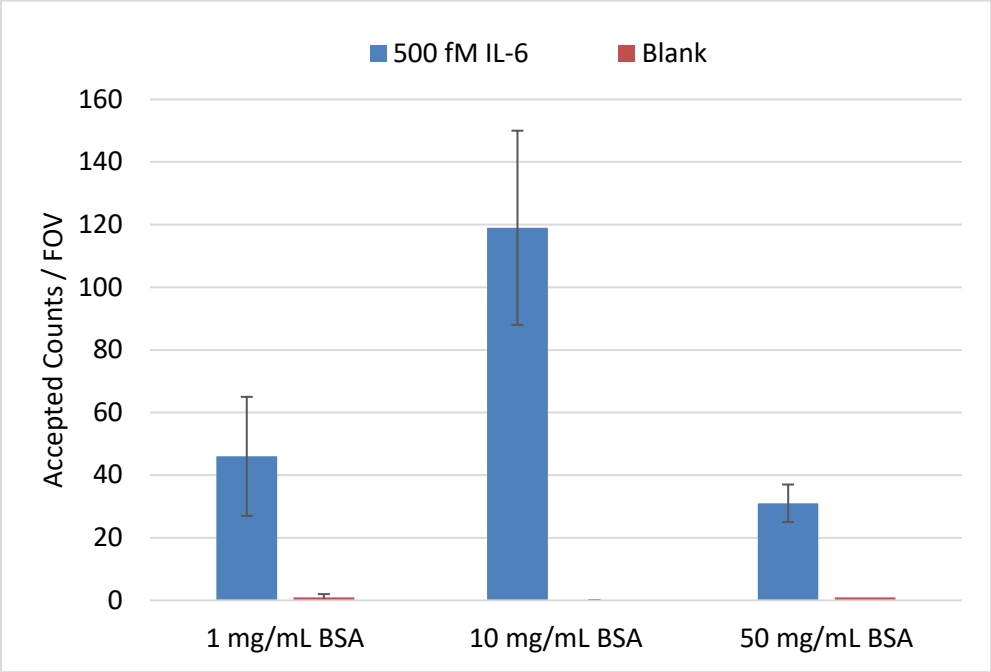

Fig. S6. Sensitivity of IL-6 detection as function of carrier BSA concentration during capture. The bar graph shows the dependence of assay sensitivity (total accepted counts per FOV after kinetic filtering at a specified concentration) as a function of carrier BSA concentration during antigen capture (IL-6) from solution. At low BSA concentration (1 mg/mL) the sensitivity is lower, presumably due to nonspecific adsorption of the antigen to the surface of the microcentrifuge tube (i.e., during sample preparation) or to the side of sample well. At 50 mg/mL, excess BSA appears to hinder the capture of antigen to the surface, reducing the sensitivity. Blue bars represent positive controls (BSA, PBS, + recombinant IL-6) and orange bars represent negative controls (BSA + PBS only). Note that this assay used non-optimized assay conditions, so the absolute number of accepted counts / FOV is not directly comparable to the final version of the assay. Error bars : 1 SEM, 2 replicate measurements.

Table S1. Summary of BLI-measured rate constants, predicted N_{b+d}, and empirically determined suitability for SiMREPS, of *in vitro*-selected candidate detection Fabs. N_{b+d} was predicted from k_{on} and k_{off} as described in Supplementary Note 2 of Johnson-Buck *et al.* (2).

Antigen	Clone Number	*In vitro* selection for fast dissociation?	k_{on} ($M^{-1}s^{-1}$)	k_{off} (s^{-1})	K_d (nM)	N_{b+d}, predicted (20 min, 50 nM probe)	Suitable for SiMREPS? (* = chosen for final assay)
IL-6	23300	N	2.98E+05	1.82E-04	0.6	0.4	N
IL-6	23312	N	5.80E+05	1.56E-03	2.7	3.6	N
IL-6	23313	N	1.41E+06	3.05E-03	2.2	7.0	N
IL-6	29805	N	7.01E+05†	4.36E-02†	62.2†	47	N
IL-6	29806	N	2.35E+06†	3.51E-02†	14.9†	65	Y*
IL-6	36299	Y	1.72E+06	1.90E-01	111	140	Y
IL-6	36300	Y	1.11E+06	3.20E-01	288	110	N
IL-6	36304	Y	7.81E+05	9.75E-02	125	67	Y
IL-6	36305	Y	2.56E+06	3.40E-01	133	220	N
PAI-1	25397	N	7.58E+05	3.28E-03	4.3	7.2	N
PAI-1	25399	N	7.79E+05	1.32E-01	170	72	N
PAI-1	25401	N	4.51E+05	6.34E-04	1.4	1.5	N
PAI-1	25402	N	6.73E+05	9.85E-03	15	18	N
PAI-1	25478	N	2.06E+06	5.43E-02	26	85	Y*
PAI-1	25483	N	2.22E+06	9.01E-02	41	120	N
IL-34	36317	Y	2.26E+05	3.85E-02	170	21	Y*
IL-34	36318	Y	9.60E+04	2.02E-02	210	9.3	N
IL-34	36319	Y	3.35E+05	2.66E-01	794	38	N
IL-34	36378	Y	8.19E+03	5.05E-02	6170	1.0	N
VEGF-A	36328	Y	4.53E+05	5.62E-02	124	39	Y
VEGF-A	36329	Y	5.42E+05	6.65E-02	123	46	Y*
VEGF-A	36380	Y	4.21E+05	8.37E-02	199	40	N
VEGF-A	36382	Y	4.04E+05	2.38E-01	589	45	Y

† For clones 29805 and 29806, BLI measurements of k_{on} were not available, so SPR-measured rate constants and K_d values are provided instead.

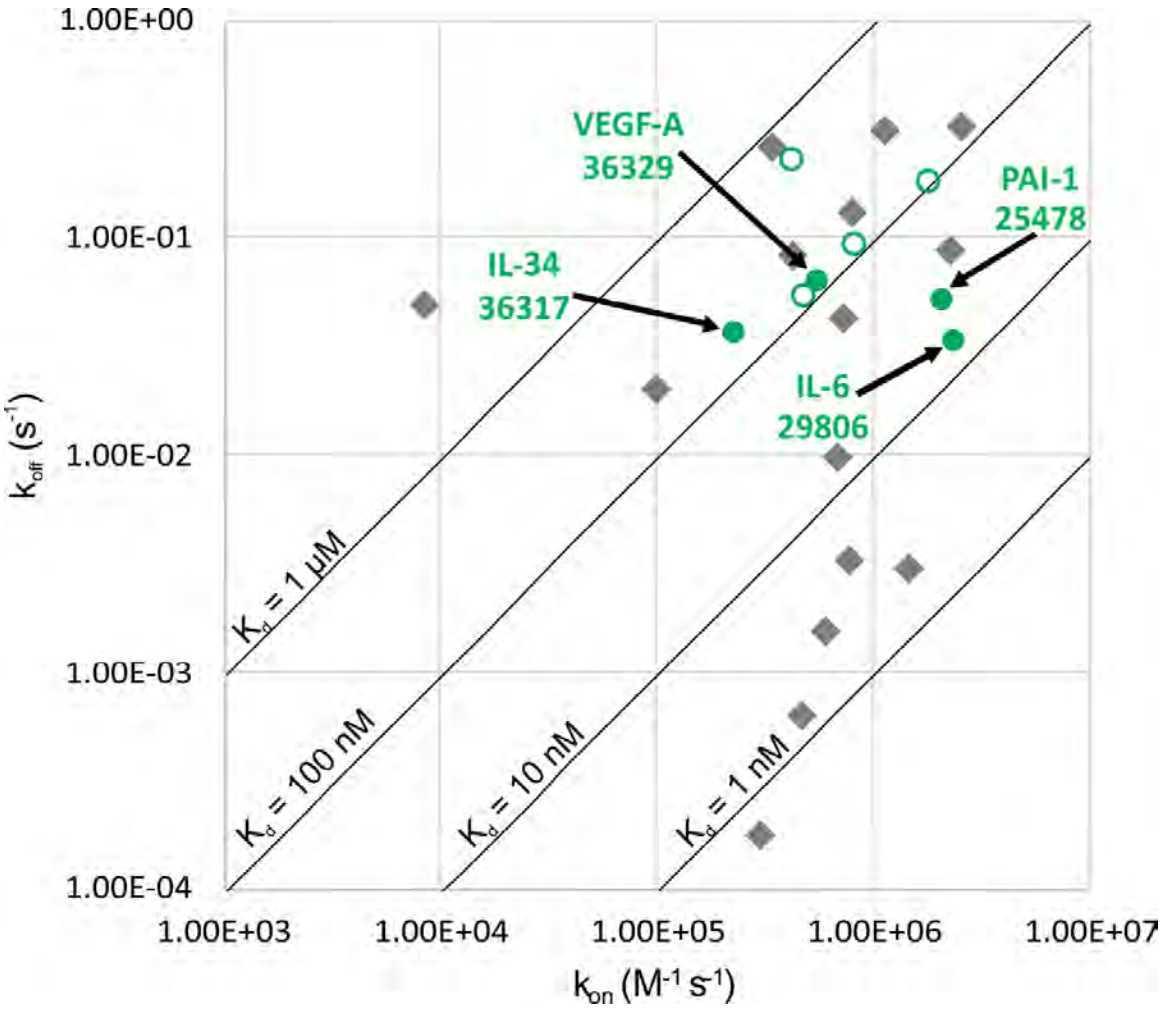

Fig. S7. Graphical representation of binding (k_{on}) and dissociation (k_{off}) rate constants (determined from BLI or SPR measurements as indicated in Supplementary Table 1) of candidate detection Fabs, with their success or failure as SiMREPS probes at room temperature indicated by color (not suitable: gray diamonds; suitable: green circles; suitable and chosen for final assays: filled green circles). IL-6 detection Fab 29806 and PAI-1 detection Fab 25478 exhibited favorable performance at room temperature, but both exhibited superior performance at elevated temperature (33-34 °C), and the PAI-1 detection Fab exhibited superior performance at room temperature but in elevated salt (500 mM Na^+).

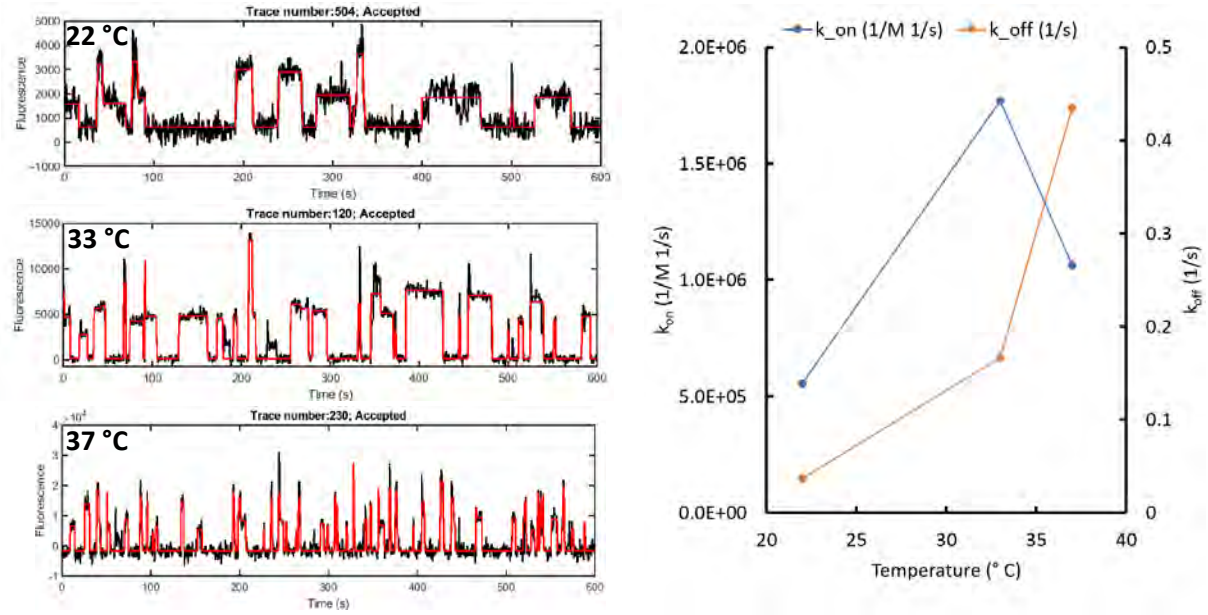

Fig. S8. Temperature dependence of binding and dissociation kinetics of IL-6 detection Fab (clone 29806). Representative intensity-versus-time traces and apparent rate constants of binding (k_{on}) and dissociation (k_{off}) of detection Fab 29806 to single surface-captured IL-6 molecules at temperatures ranging from 22 °C to 37 °C. The k_{off} increases by more than 10-fold with increasing temperature, enabling the observation of more binding and dissociation events in the same amount of time (or, equivalently, the same number of binding events in a shorter period of time). Apparent k_{on} and k_{off} values were determined from single-exponential fitting of cumulative dwell time distributions from at least 50 single-molecule traces.

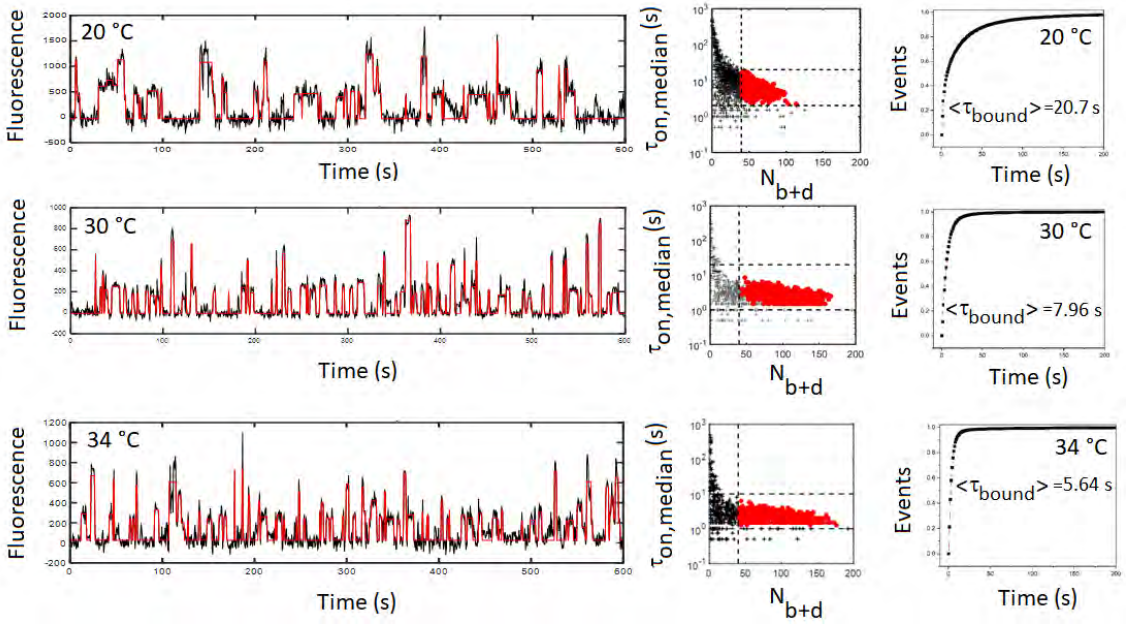

Fig. S9. Temperature dependence of binding and dissociation kinetics of PAI-1 detection Fab (clone 25478). Representative intensity-versus-time traces, N_{b+d} *versus* $\tau_{bound,median}$ scatter plots, and bound-state dwell time distributions fit with single-exponential decay functions to determine k_{off} of detection Fab 25478 binding to surface-captured PAI-1 molecules at temperatures ranging from 20 °C to 34 °C. The k_{off} increases 3- to 4-fold with increasing temperature from 20 to 34 °C, enabling the observation of more binding and dissociation events in the same amount of time (or, equivalently, the same number of binding events in a shorter period of time). Apparent k_{off} values were determined from single-exponential fitting of cumulative dwell time distributions from at least 300 single-molecule traces.

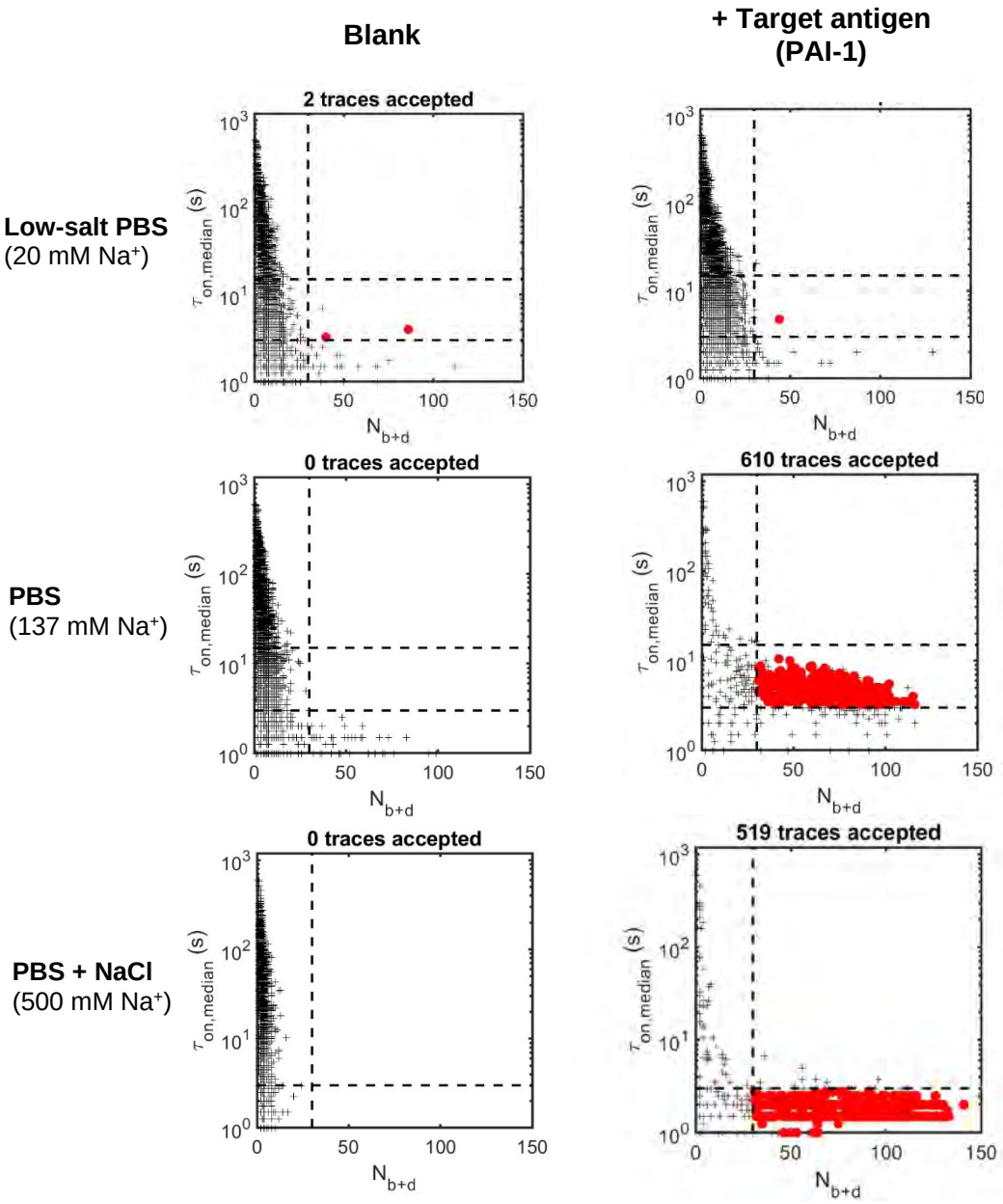

Fig. S10. Salt dependence of binding and dissociation kinetics of PAI-1 detection Fab (clone 25478). Increasing sodium ion concentration in the imaging buffer suppresses background binding and accelerates dissociation of the detection Fab for PAI-1. N_{b+d}-versus-$\tau_{on,median}$ plots show that, as sodium ion concentration is increased from 20 mM to 500 mM, the N_{b+d} values in the blank measurement become smaller on average, indicating less background binding of the detection probe to the assay surface. Simultaneously, as sodium ion concentration is increased, the median bound-state lifetime of the query probe decreases, and the average N_{b+d} value observed in the presence of the target antigen PAI-1 increases. The combination of lower nonspecific binding and faster dissociation from the antigen results in kinetics of specific and nonspecific binding that are more easily distinguished at higher salt concentrations.

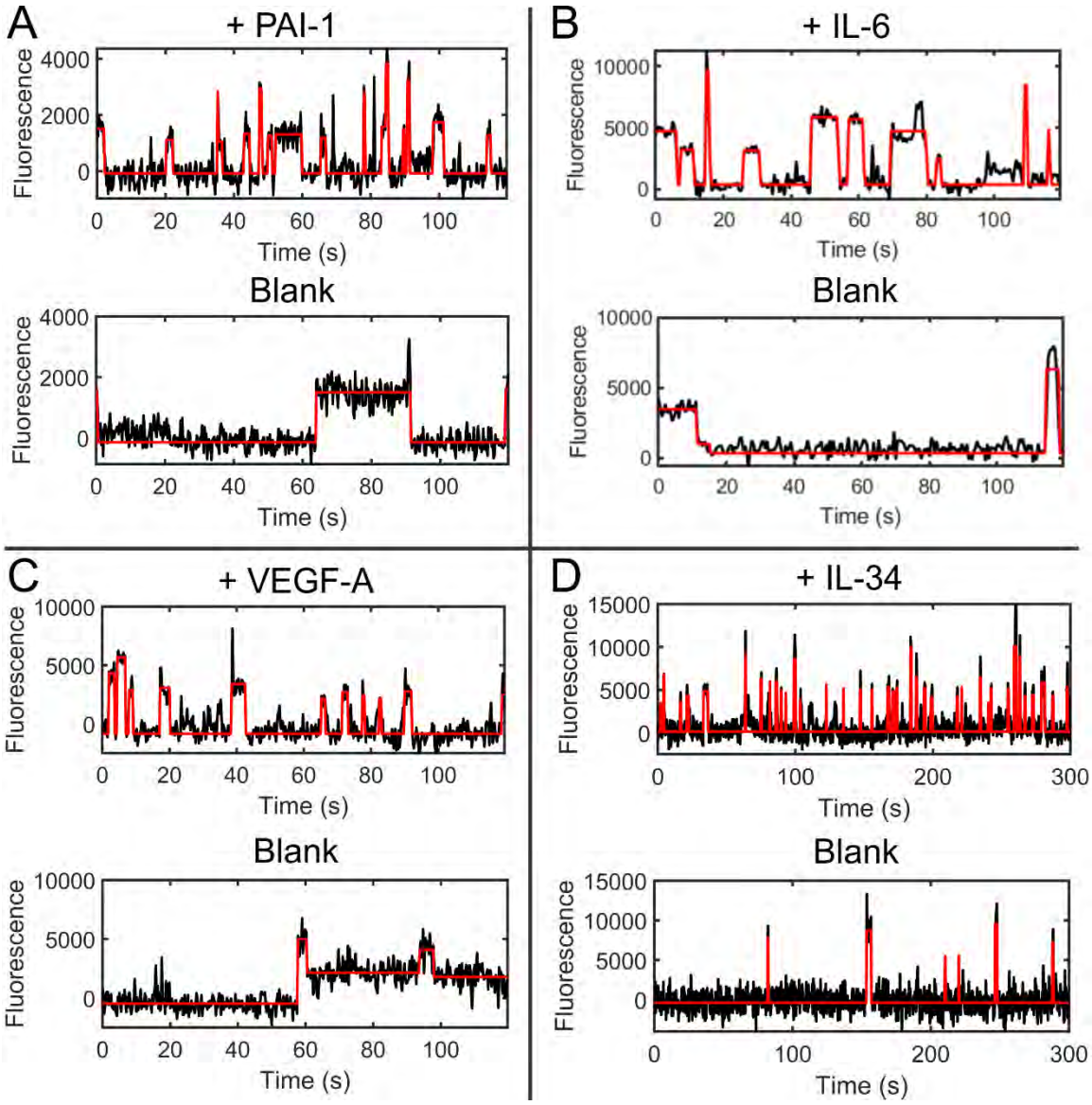

Fig. S11. Representative single-molecule traces from the final versions of the four SiMREPS assays developed in this work. a, b, c, d, Single-molecule intensity-*versus*-time traces for assays of PAI-1 (*A*), IL-6 (*B*), VEGF-A (*C*), and IL-34 (*D*) in either the presence or absence of the target antigen. Raw intensity values (black line) and the corresponding HMM idealization (red line) used for kinetic analysis are shown. All traces were collected in a matrix of 25% animal serum.

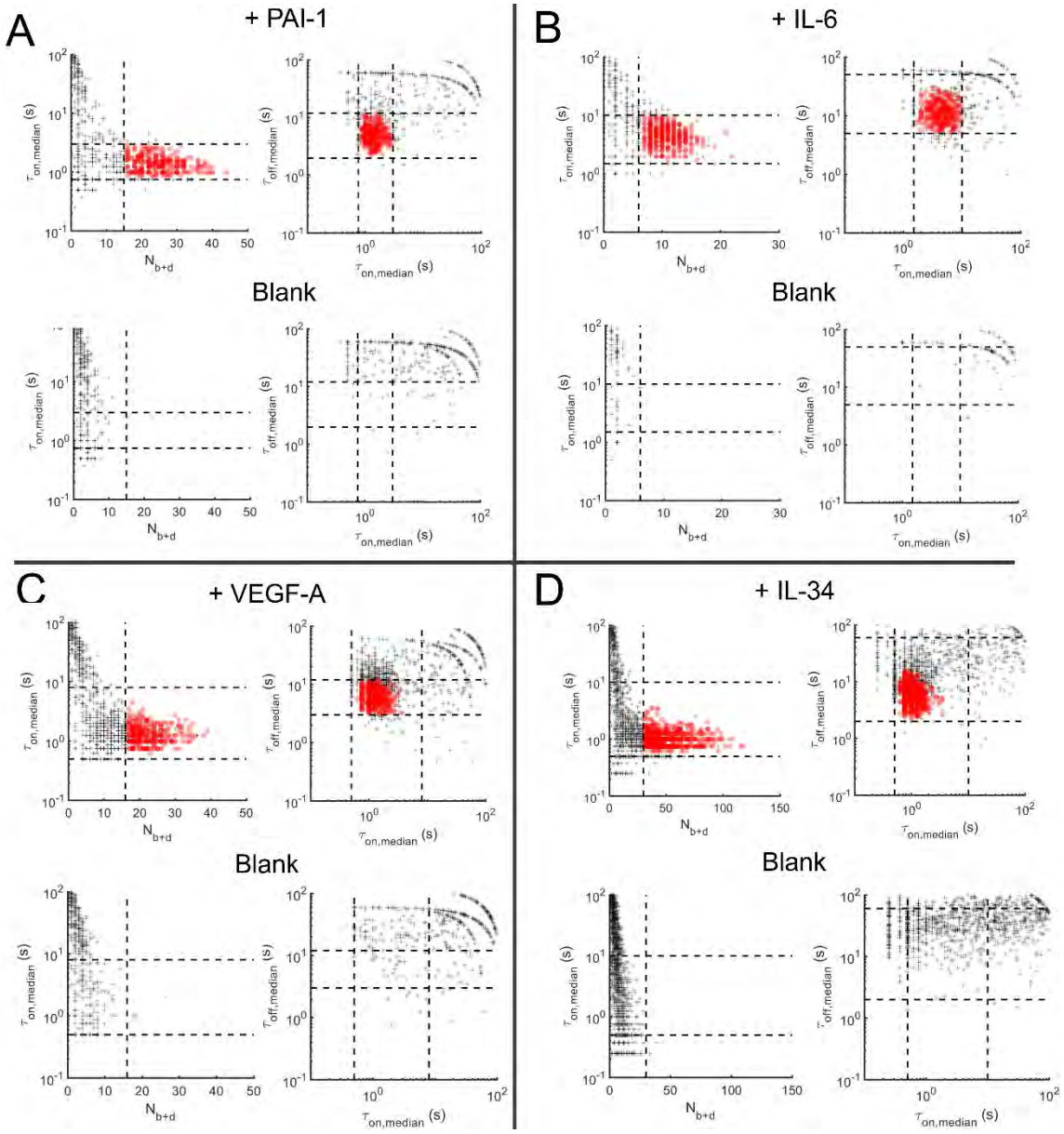

Fig. S12. Representative kinetics plots and filtering thresholds for the final versions of the four SiMREPS assays developed in this work. *A, B, C, D*, Scatter plots of the number of binding and dissociation events (N_{b+d}), median bound-state lifetime ($\tau_{on,median}$), and median unbound-state lifetime ($\tau_{off,median}$) from all traces detected within a single representative field of view for assays of PAI-1 (*A*), IL-6 (*B*), VEGF-A (*C*), and IL-34 *(D*). Each point in the scatter plots represents a candidate single-molecule trace. Dashed lines represent threshold values (minima and/or maxima) for accepting a trace as a positive detection event for the antigen. Red circles represent accepted traces (i.e., those classified as positive detection events), while black crosses represent traces that were rejected based on intensity, signal-to-noise, or kinetic criteria. Threshold values for the four assays are listed in Table S2.

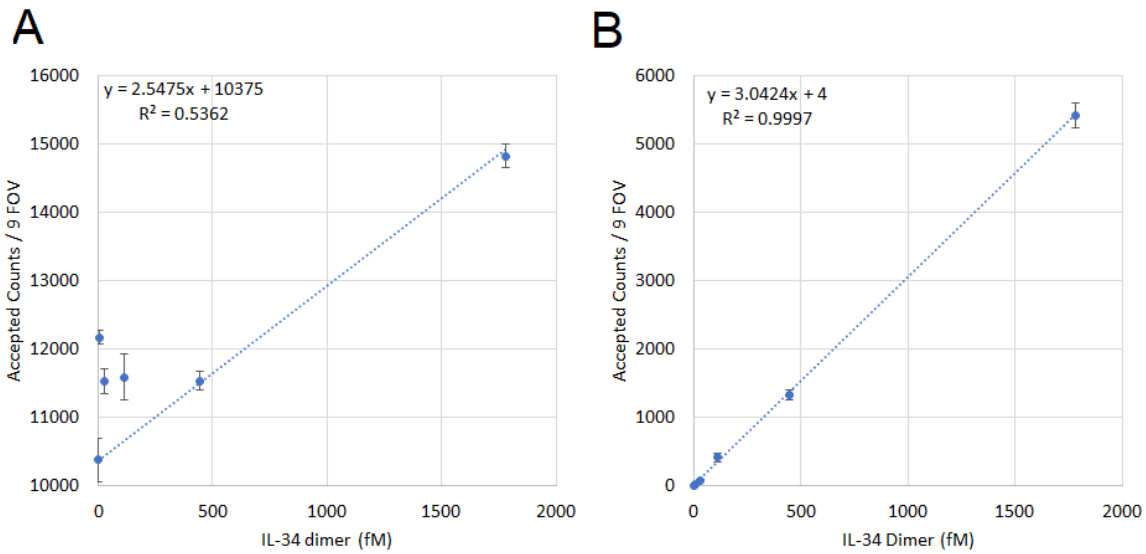

Fig. S13. Kinetic filtering is critical for quantitative and sensitive measurement in SiMREPS. (*A*) Standard curve of IL-34 without kinetic filtering (Intensity + S/N only) gives a limit of detection (LOD) of 340 fM (20 pg/mL) and (*B*) Standard curve with kinetic filtering gives much lower LOD of 1.7 fM (0.089 pg/mL).

Table S2. Acquisition parameters and kinetic filtering criteria for optimized SiMREPS assays of each antigen.

	IL-6	**IL-6 (super-resolution analysis** (3)**)**	**PAI-1**	**VEGF-A**	**IL-34**
Detection probe AbD clone #	29806	29806	25478	36329	36317
Detection probe concentration (nM)	50	50	50	50	50
Exposure time per frame (s)	0.5	0.5	0.25	0.25	0.25
Acquisition time (min)	2	2	2	2	5
Acquisition temperature (°C)	33.5	33.5	22	22	22
Minimum $r_{s/n}$ per event	3	4	2.5	2	3
Minimum $r_{s/n}$ per trace	3	-	2.5	4	3
Minimum N_{b+d}	6	6	15	16	30
Minimum $\tau_{on,median}$ (s)	1.5	1.5	0.75	0.5	0.5
Maximum $\tau_{on,median}$ (s)	10	-	2	8	10
Minimum $\tau_{off,median}$ (s)	5	5	3	3	2
Maximum $\tau_{off,median}$ (s)	50	-	12	12	60
Maximum $\tau_{off,max}$ (s)	60	60	50	100	-
Maximum σ_x, σ_y (pixels)	-	0.75	-	-	-

NOTES: Super-resolution analysis cannot evaluate a signal-to-noise ratio throughout an entire trace in the same way that diffraction-limited analysis can, since events are evaluated individually rather than as a single intensity time series; furthermore, maximum values of the median bound- and unbound-state lifetimes are not applied in super-resolution analysis to avoid false negatives that might be caused by the algorithm missing a single binding or dissociation event. Maximum positional standard deviations (σ_x, σ_y) per candidate molecule are only relevant for super-resolution analysis, and are used to ensure that all clustered binding and dissociation events are likely to originate from the same analyte molecule.

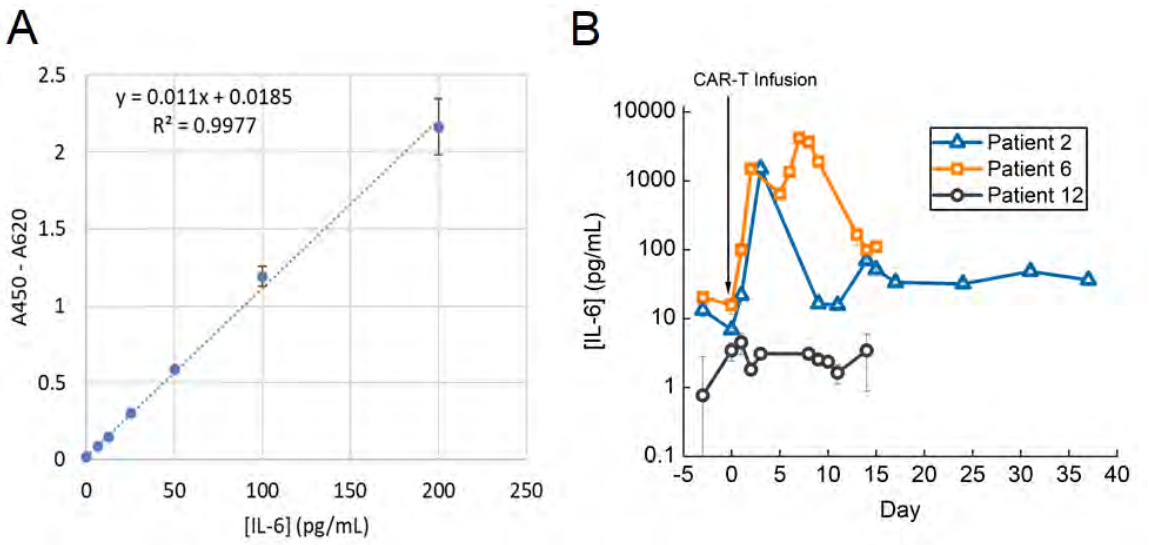

Fig. S14. Time course IL-6 measurements in CAR-T patient serum by sandwich ELISA. (*A*) ELISA standard curve used for quantification of IL-6 in serum samples of CAR-T therapy patients. (*B*) Time course of IL-6 concentration as measured by ELISA in serum samples from three CAR-T therapy patients who experienced maximum CRS grades of 4 (Patient 6, orange squares), 2 (Patient 2, blue triangles), or 0 (Patient 12, black circles) during the sample collection window. Samples were measured at either 4-fold or 64-fold dilution. Error bars: Standard deviation from 2 replicates.

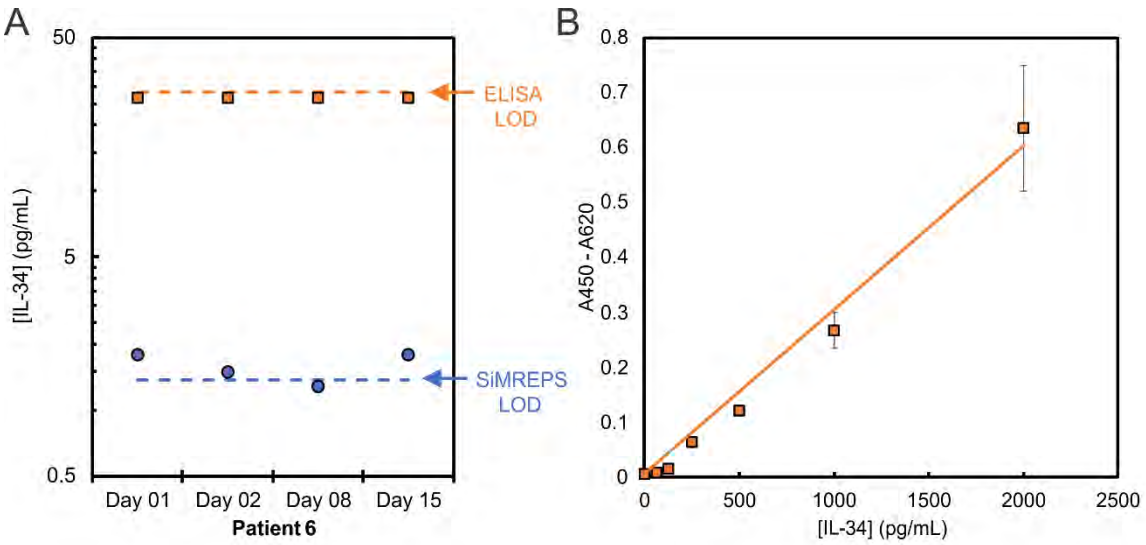

Fig. S15. Attempted detection of IL-34 in CAR-T patient serum by SiMREPS and sandwich ELISA. (*A*) SiMREPS detects significant concentrations of IL-34 in three of four tested serum specimens from CAR-T patient number 6; by contrast, ELISA (orange squares) does not detect significant levels of IL-34 in any of the four specimens. Specimens include those collected 1, 2, 8, or 15 days after CAR-T infusion, as indicated, and correspond to time points at which IL-6 concentration varied by approximately two orders of magnitude. (*B*) Standard curve used in the quantification of IL-34 by ELISA provides a positive control indicating that the ELISA reagents were functional. Error bars are one standard deviation from two replicates.

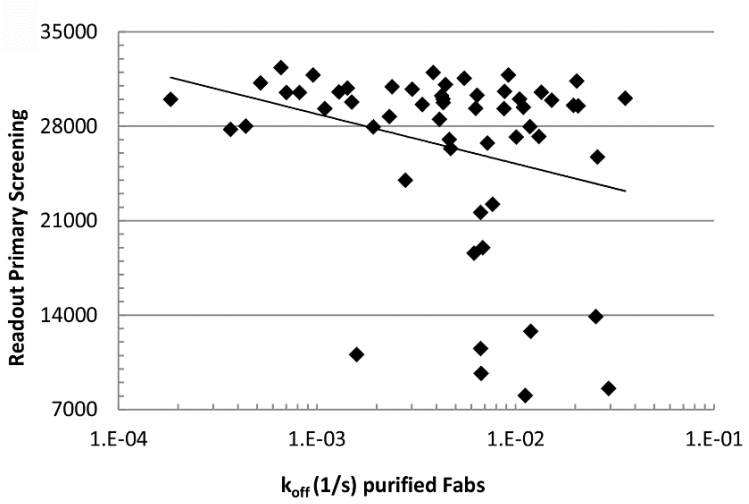

Fig. S16. Selection by phage display yields many Fabs with rapid dissociation kinetics. In a prior study, the dissociation rate k_{off} was determined for all hits found in a standard phage display selection against the drug cetuximab (4). Clones with k_{off} values ideal for ELISA are rare, whereas over a dozen clones exhibited dissociation rate constants that would make them promising candidates for SiMREPS (k_{off} between 0.01 and 0.1 s^{-1}). Reprinted from ref. (4), which is licensed under CC BY 3.0.

Supplementary References

1. B. Hua, *et al.*, An improved surface passivation method for single-molecule studies. *Nat Methods* **11**, 1233–1236 (2014).

2. A. Johnson-Buck, *et al.*, Kinetic fingerprinting to identify and count single nucleic acids. *Nat Biotechnol* **33**, 730–732 (2015).

3. S. L. Hayward, *et al.*, Ultraspecific and amplification-free quantification of mutant DNA by single-molecule kinetic fingerprinting. *J Am Chem Soc* **140**, 11755–11762 (2018).

4. F. Ylera, S. Harth, D. Waldherr, C. Frisch, A. Knappik, Off-rate screening for selection of high-affinity anti-drug antibodies. *Anal Biochem* **441**, 208–213 (2013).